The Longitudinal Spin Structure of the Nucleon

A 12 GeV Research Proposal to Jefferson Lab (PAC 30)

Moskov Amarian, Stephen Bültmann, Gail Dodge, Nevzat Guler, Henry Juengst, Sebastian Kuhn[†*], Lawrence Weinstein
Old Dominion University

Harut Avakian, Peter Bosted, Volker Burkert, Alexandre Deur[†], Vipuli Dharmawardane[†]
Jefferson Lab

Keith Griffioen[†]
The College of William and Mary

Hovanes Egiyan, Maurik Holtrop[†]
University of New Hampshire

Stanley Kowalski, Yelena Prok[†]
Massachusetts Institute of Technology

Don Crabb[†], Karl Slifer
University of Virginia

Tony Forest[†]
Louisiana Tech

Angela Biselli
Fairfield University

Kyungseon Joo
University of Connecticut

Mahbub Khandaker
Norfolk State University

Elliot Leader
Imperial College, London, England

Aleksander V. Sidorov
Bogoliubov Theoretical Laboratory, JINR Dubna, Russia

Dimiter B. Stamenov
Inst. for Nuclear Research and Nuclear Energy, Bulgarian Academy of Sciences, Sofia, Bulgaria

A CLAS collaboration proposal

[†] Co-spokesperson [*] Contact: Sebastian Kuhn, Department of Physics, Old Dominion University, Norfolk VA 23529. Email: skuhn@odu.edu

Collaborators' commitment to the 12 GeV upgrade of Jefferson Lab

- The Old Dominion University group (Prof. Amarian, Bültmann, Dodge, Kuhn and Weinstein) is actively involved in this proposal, as well as two other proposal using CLAS12. Other members of our group are pursuing a proposal for Hall A, but their contributions are not included here. Among CLAS12 baseline equipment, the group intends to take responsibility for the design, prototyping, construction and testing of the Region 1 Drift Chamber. Five faculty (including one research faculty) and one technician are likely to work at least part time on this project in the next few years. Funding for the group is from DOE and from the university (75% of research faculty salary + one regular faculty summer salary + 50% of the technician). The university has also provided 6000 square feet of high bay laboratory space with clean room capabilities for our use. We will seek other sources of funding as appropriate. Gail Dodge is the chair of the CLAS12 Steering Committee and the user coordinator for the CLAS12 tracking technical working group. Beyond the baseline equipment, the group is also interested in exploring improvements to the BoNuS detector and a future RICH detector for CLAS12.

- The UNH group is committed to significant contributions in the development of the CLAS12 software. Maurik Holtrop is currently chair of the CLAS12 GEANT4 simulation group to which our post-doc Hovanes Egiyan is also contributing. Since currently the main software efforts for CLAS12 are in the area of simulation we are also part of and contributing to the general CLAS12 Software group. Current man power commitments to this effort are 0.15 FTE of a faculty and 0.4 FTE of one post-doc. We expect to increase this effort as our CLAS activities wind down and our CLAS12 activities pick up and we expect to attract some talented undergraduate students to this project. These efforts are funded from our current grant with DOE. In addition to the software efforts the UNH group is planning to contribute to the prototyping and construction of the silicon vertex detector. No formal agreements have been made on this effort yet and no addition grants have been written yet. However, it is expected that we will be able to attract additional funding for this project with which we will fund an additional post-doc and one or two undergraduate students. One of the faculty from the UNH Space Science Center, Jim Connel, a cosmic ray experimentalist with a background in nuclear physics, is very interested in joining the vertex detector project. He has considerable experience with silicon detectors for space observations.

- The UConn group has made a commitment to help build the CLAS12 high threshold cerenkov counter (HTCC) with Youri Sharabian and the RPI group. Early this year our group got funding of $65,000 ($32,500 from UConn and $32,500 from JLab) to build a HTCC prototype. Also UConn is providing 1/2 postdoctoral support for Maurizio Ungaro for the next two years and commits to support 1/2 graduate student for 1 year for the CLAS12 upgrade efforts. Our group of one PI, one postdoc and 4 graduate students will provide substantial manpower towards the 12 GeV upgrade. Recently we got a DOE STTR Phase I grant to build a software framework for data archiving and data analysis for nuclear physics experiment with one UCon computer science professor and a local software company. With this grant, we expect to contribute to software development for the 12 GeV upgrade.

- The College of William and Mary group is actively involved in this proposal, as well as several other proposals using CLAS12. Other members of our group are also pursuing a proposal for Hall A, but their contributions are not included here. Among CLAS12 baseline equipment, the group is committed to building part of the forward tracking system, but the exact tasks have not yet been determined. At least one faculty member, two graduate students, half a post-doc and several undergraduates are likely to work at least part time on this project in the next few years. Funding for the group is from the DOE and from the NSF. Additional funding will be sought for building the base equipment. Facilities at William and Mary include a clean room suitable for drift-chamber construction, and, on the time scale of a few years in the future, ample space for detector construction and testing.

- The University of Virginia Polarized Target Group is actively involved in this proposal as well as other proposals using CLAS12. Some members of the group are also involved in proposals for Hall C. The group's contribution to the CLAS12 baseline equipment will be the design, construction and testing of the longitudinal polarized target discussed in this proposal. The target will use a horizontal ^{4}He evaporation refrigerator with a conventional design and similar to ones built and operated in the past. The refrigerator will be constructed in the Physics Department workshop; the workshop staff have experience with building such devices. Testing will be done in our lab where all the necessary infrastructure is on hand. Two Research Professors (75% of salary from UVA, 17% from DOE), two Post-Docs and two graduate students, all supported by DOE, will spend their time as needed on this project. Other funding will be pursued as necessary. Outside the base equipment considerations one member of the group (DGC) has started working with Oxford Instruments on a design for an optimized transverse target magnet to be used for transverse polarization measurements with CLAS12.

Abstract

We are proposing a comprehensive program to map out the x- and Q^2-dependence of the helicity structure of the nucleon in the region of moderate to very large x where presently the experimental uncertainties are still large. The experiment will use the upgraded CLAS12 detector, 11 GeV highly polarized electron beam, and longitudinally polarized solid ammonia targets (NH_3 and ND_3). Thanks to the large acceptance of CLAS12, we will cover a large kinematical region simultaneously. We will detect both the scattered electrons and leading hadrons from the hadronization of the struck quark, allowing us to gain information on its flavor. Using both inclusive and semi-inclusive data, we will separate the contribution from up and down valence and sea quarks in the region $0.1 \leq x \leq 0.8$. These results will unambiguously test various models of the helicity structure of the nucleon as $x \to 1$. A combined Next-to-Leading Order (NLO) pQCD analysis of our expected data together with the existing world data will significantly improve our knowledge of all polarized parton distribution functions, including for the gluons (through Q^2–evolution). High statistics data on the deuteron in the region of moderate x and with a fairly large range in Q^2 are crucial for this purpose. Finally, we will be able to improve significantly the precision of various moments of spin structure functions at moderate Q^2, which will allow us to study duality and higher-twist contributions.

We request 30 days of running on NH_3 and 50 days of running on ND_3 (or possibly ^{6}LiD), including about 20% overhead for target anneals, polarization reversal, and auxiliary measurements.

Contents

1 Introduction

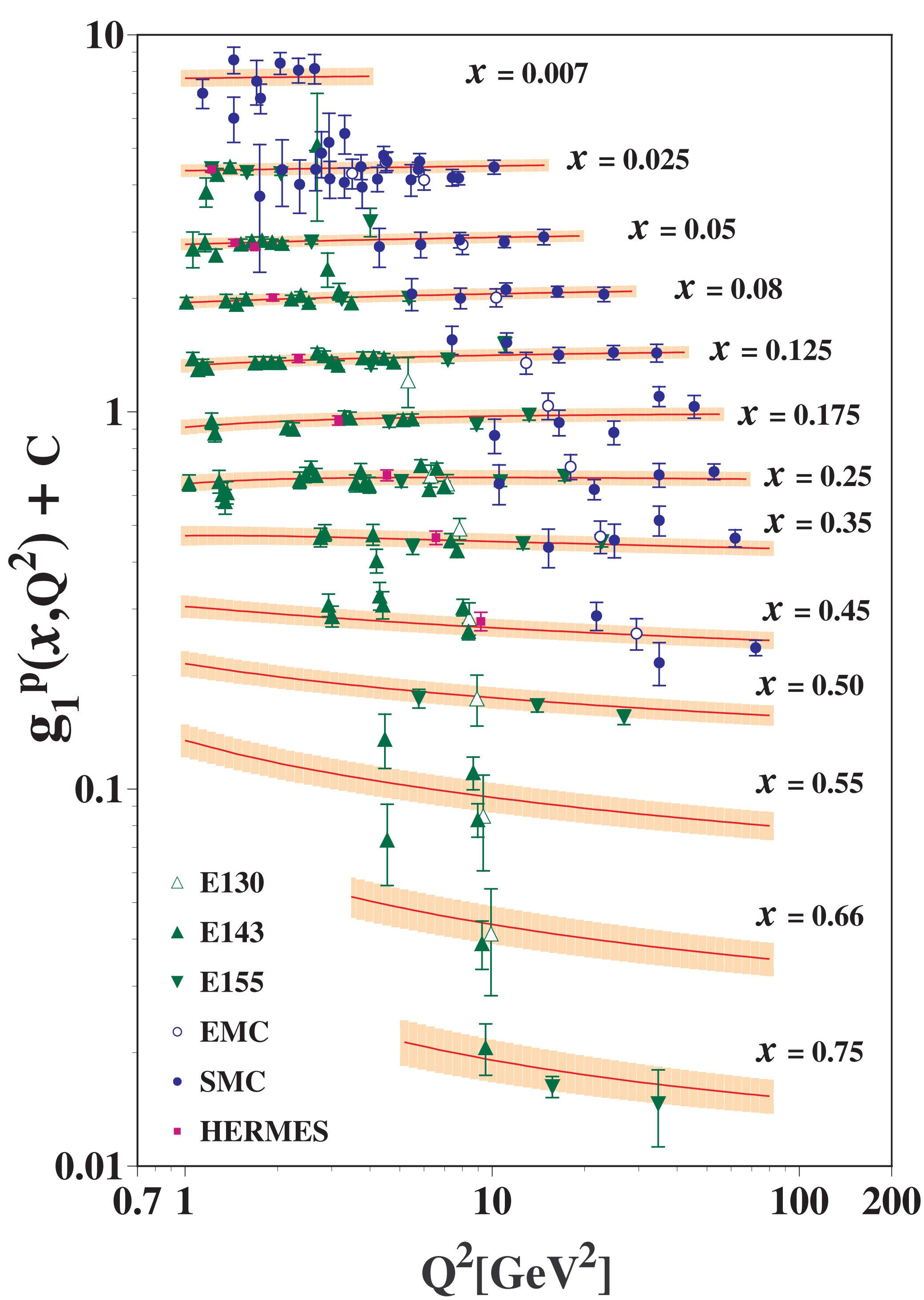

Figure 1: A sample of the existing world data on the spin structure function g_1, compiled by the AAC collaboration [1].

Spin structure functions of the nucleon have been measured in deep inelastic (DIS) lepton scattering for nearly 30 years. A sample of these data for the proton is shown in Fig. 1. After the first experiments at SLAC [2], interest in this topic was magnified in the 80's when the EMC collaboration found [3] that the quark helicities made only a small contribution to the overall helicity of the proton. This "spin crisis" led to a very vigorous theoretical and experimental effort over the next 20 years, with a large data set collected at CERN, SLAC, DESY and Jefferson Lab [4, 5, 6, 7, 8, 9, 10, 11, 12]. As of today, the data indicate that approximately 25% - 35% of the nucleon spin is carried by the quark spins, with the remainder having to come from gluon polarization and orbital angular momentum. It remains an open question whether at least the three valence quark spins (uud in the proton) follow the "naive" expectation of relativistic quark models (60% – 70% of the nucleon spin carried by quark helicities).

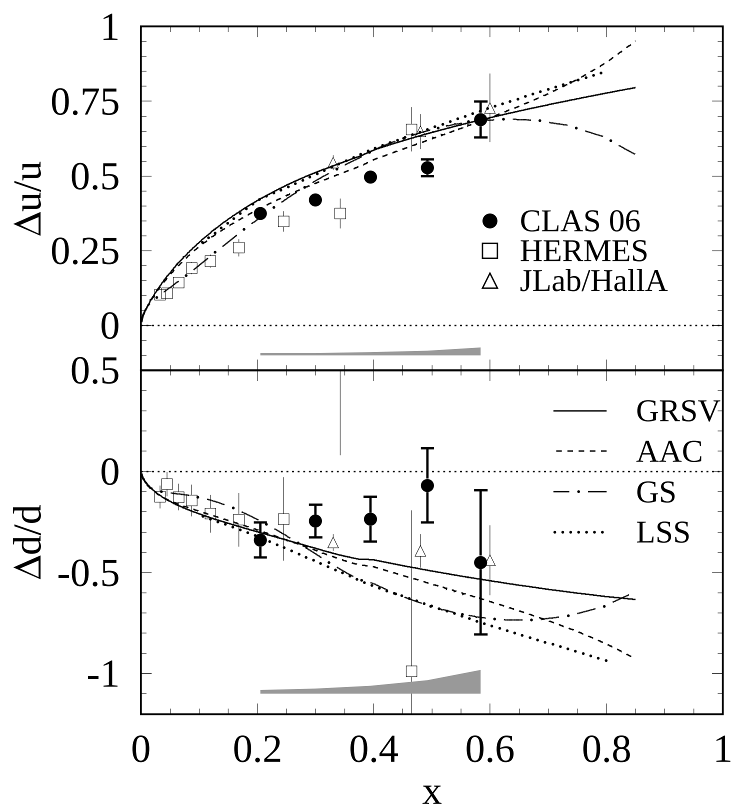

Figure 2: Approximate polarization of the valence up and down quarks in the proton extracted from recent JLab experiments on the virtual photon asymmetry A_1 for the proton, deuteron and neutron (^{3}He).

The interest in this field continues unabated as new experiments (COMPASS at CERN [13] and the nucleon spin program at RHIC [14]) are attempting to measure the low-x gluon and sea quark polarization in a polarized nucleon with high precision. At the other end of the spectrum, new data from JLab [12, 15] address for the first time the question of the helicity structure of the nucleon at large x, where sea quark and gluon contributions are minimal and measurements are mostly sensitive to valence quarks. Examples of these results are shown in Fig. 2.

However, to fully access the region of high x and moderate Q^2, one needs higher beam energies than presently available at JLab. In particular, to test various models of the asymptotic value of the virtual photon asymmetry $A_1(x)$ as $x \to 1$, one needs the upgraded CEBAF with 11 GeV beam energy. In addition, the very high luminosity combined with large acceptance detectors required to extract statistically significant results will only be available at Jefferson Lab for the foreseeable future. In this proposal, we are describing an experiment to be conducted with highly polarized 11 GeV electron beam in Hall B, the upgraded CLAS12 detector, and longitudinally polarized proton and deuteron targets to fully explore this physics. A companion experiment with transversely polarized targets in CLAS12 (to be proposed to a future PAC) will address additional topics of high interest and will help to minimize systematic errors of the present proposal.

In addition to directly accessing the quark helicities in the limit $x \to 1$, the comprehensive data set to be collected by the proposed experiment, covering a large kinematic range in x and Q^2, will contribute significantly to our knowledge of polarized parton distribution functions for all quark flavors and even the polarized gluon distribution Δg. Through Next-to-Leading Order (NLO) analyses of the world data on inclusive DIS (using the DGLAP evolution equations), one can constrain these distribution functions and their integrals. Existing CLAS data from 6 GeV running already have an impact on these fits. The expected data from the proposed experiment at 11 GeV will yield further dramatic reductions in the errors on these distributions. In addition, we will also collect semi-inclusive DIS (SIDIS) data, where in addition to the scattered electron, we will detect some of the leading hadrons produced when the struck quark hadronizes. These data will further constrain the NLO fits and improve the separation of the various quark flavors' contribution to the nucleon spin.

A final objective of the proposed measurement is to augment existing spin structure function data at low to moderate Q^2 for the precise evaluation of various moments of g_1. In particular, high precision data from CLAS and Hall A exist at Q^2 below about 3 GeV^2 (see Fig. 3). However, at the higher Q^2 a significant fraction of these moments (at small x) are not measured directly in the JLab experiments and these contributions are instead approximated using a fit to other existing data (mostly in the DIS region). Using the 11 GeV beam, we can increase considerably the low-x coverage for the highly precise JLab data and therefore get a more reliable determination of these moments. In turn, these moments at moderate Q^2 are very useful to study issues like higher twist contributions to the nucleon spin structure, such as quark-gluon correlations and the polarizability of the chromo-electric and chromo-magnetic gluon field in the nucleon. Our data will also allow us to quantify further to what extent quark-hadron duality is present in inclusive spin structure functions, by supplying a reliable set of spin structure functions in the high-x DIS region to compare to measurements in the resonance region.

In the remainder of this document, we will explain each of these Physics objectives in more detail, describe the experimental technique, and show expected results, followed by our beam time request. Necessary conventions and definitions that are used throughout this

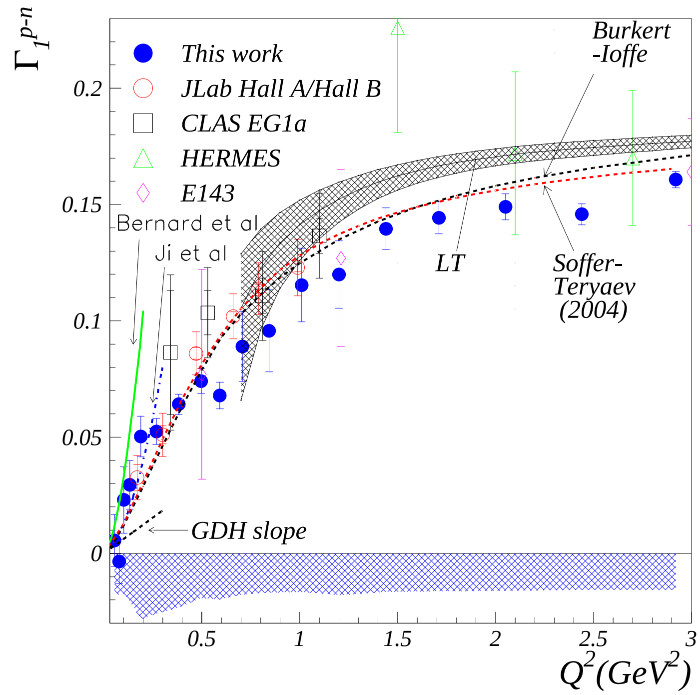

Figure 3: Recent results on the Bjorken Integral from Hall A and CLAS.

document are introduced in the following paragraph:

The kinematics of the scattered electron (of initial energy E) is described by its energy E', the energy transferred to the target $\nu = E - E'$, the three-momentum transferred $\vec{q} = \vec{p}_{el} - \vec{p}\,'_{el}$ and the four-momentum transferred $Q^2 = \vec{q}^{\,2} - \nu^2 = 4EE' \sin^2 \theta_{el}/2$ as well as the Bjorken variable $x = Q^2/2m_p\nu$ which measures the fraction of the nucleon momentum carried by the struck quark. The invariant mass of the unobserved final state in inclusive scattering (e, e') is given by $W = \sqrt{m_p^2 + 2m_p\nu - Q^2}$. In semi-inclusive processes (SIDIS), we also observe a pion or kaon in the final state that carries the fraction $z = E_h/\nu$ of the photon energy and has a momentum component p_T transverse to the direction of the virtual photon. In all cases, we measure the number of events for antiparallel (N^+) and parallel (N^-) electron and target spins. The normalized asymmetry $A_{||} = (N^+ - N^-)/(N^+ + N^-)$ is corrected for backgrounds, QED radiative effects and beam and target polarization and can be related to the virtual photon asymmetries A_1 and A_2 via

$$A_{||} = D(A_1(x, Q^2) + \eta A_2(x, Q^2)), \tag{1}$$

where

$$D = \frac{1 - \epsilon E'/E}{1 + \epsilon R}, \eta = \frac{\epsilon Q}{E - \epsilon E'}, \epsilon = \left(1 + 2\frac{\vec{q}^{\,2}}{Q^2} \tan^2 \frac{\theta_{el}}{2}\right)^{-1}, \tag{2}$$

and R is the ratio of longitudinal to transverse virtual photon absorption cross section. The asymmetries A_1 and A_2 are related to the polarized spin structure functions g_1 and g_2 via

$$A_1F_1(x,Q^2) = g_1(x,Q^2) - \frac{Q^2}{\nu^2}g_2(x,Q^2), A_2F_1(x,Q^2) = \frac{Q}{\nu}(g_1(x,Q^2)+g_2(x,Q^2)), \qquad (3)$$

where F_1 is the unpolarized structure function.

2 Physics Motivation and Existing Data

In the following, we will outline the main topics addressed by the proposed experiment and explain how new data can significantly improve upon the present state of knowledge.

2.1 Nucleon Helicity Structure at Large x

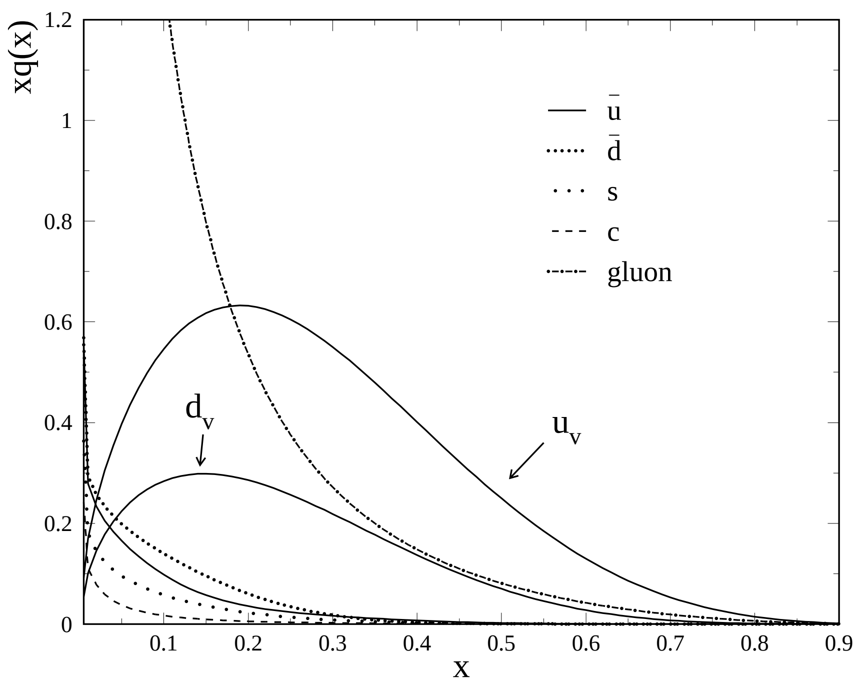

Figure 4: Parton distributions at $Q^2 = 8$ GeV^2 in CTEQ6M parameterization.

One of the most fundamental properties of the nucleon is the structure of its valence quark distributions. Valence quarks are the irreducible kernel of each hadron, responsible for its charge, baryon number and other macroscopic properties. The region $x \to 1$ is a relatively clean region to study the valence structure of the nucleon since this region is dominated by valence quarks while the small x region is dominated by gluon and sea densities (Fig. 4). Due to its relative Q^2-independence in the DIS region, the virtual photon asymmetry A_1, which is approximately given by the ratio of spin-dependent to spin averaged structure functions,

$$A_1(x) \approx \frac{g_1(x)}{F_1(x)}, \qquad (4)$$

is one of the best physics observables to study the valence spin structure of the nucleon. At leading order,

$$A_1(x, Q^2) = \frac{\sum e_i^2 \Delta q_i(x, Q^2)}{\sum e_i^2 q_i(x, Q^2)}, \tag{5}$$

where $q = q \uparrow + q \downarrow$ and $\Delta q = q \uparrow - q \downarrow$ are the sum and difference between quark distributions with spin aligned and anti-aligned with the spin of the nucleon. The x dependence of the parton distributions provide a wealth of information about the quark-gluon dynamics of the nucleon. in particular spin degrees of freedom allow access to information about the structure of hadrons not available through unpolarized processes. Furthermore, the spin dependent distributions are more sensitive than the spin-averaged ones to the quark-gluon dynamics responsible for spin-flavor symmetry breaking. Several models make specific predictions for the large x behavior of quark distributions. However, the deep valence region, at $x > 0.6$, lacks high precision measurements for the spin-dependent quark distributions. This situation can be greatly improved by the 11 GeV beam, polarized NH_3 and ND_3 targets and the CLAS12 detector in Hall B.

2.1.1 Predictions for A_1 at large x

SU(6) quark model

One of the simplest models for A_1 is the SU(6) quark model. In the exact SU(6) symmetry the proton wave function is given by,

$$\begin{aligned} p \uparrow = \; & \tfrac{1}{\sqrt{2}} u \uparrow (ud)_{S=0} + \tfrac{1}{\sqrt{18}} u \uparrow (ud)_{S=1} - \tfrac{1}{3} u \downarrow (ud)_{S=1} \\ & - \tfrac{1}{3} d \uparrow (uu)_{S=1} - \tfrac{\sqrt{2}}{3} d \downarrow (uu)_{S=1}, \end{aligned}$$

where S denotes the total spin of the diquark component. The neutron wave function can be obtained by interchanging u and d in the proton wave function. In the exact SU(6) symmetry, $S = 0$ and $S = 1$ di-quark configurations are equi-probable, leading to the predictions,

$$A_1^p = \frac{5}{9}; \qquad A_1^n = 0; \qquad \frac{d}{u} = \frac{1}{2}; \qquad \frac{\Delta u}{u} = \frac{2}{3}; \qquad \frac{\Delta d}{d} = -\frac{1}{3}.$$

Existing data on A_1, in particular newly published Hall-B results [15] and existing Hall-A neutron results [12], already exceed the SU(6) predictions at large x.

Hyperfine perturbed quark model

In the hyperfine-perturbed quark model SU(6) symmetry is explicitly broken by introducing hyperfine interactions [16], H_{hyp}, between each pair of quarks (i, j), which is of the form [17],

$$H_{hyp}^{ij} = A \left[\frac{8\pi}{3} \delta^3(\vec{r_{ij}}) \vec{S_i} \cdot \vec{S_j} + \frac{1}{r_{ij}^3} (3\vec{S_i} \cdot \hat{r}_{ij} \vec{S_j} \cdot \hat{r}_{ij} - \vec{S_i} \cdot \vec{S_j}) \right], \tag{6}$$

where $\vec{S_i}$ is the spin of the i^{th} quark, $\vec{r_{ij}}$ is a vector joining the i^{th} and j^{th} quark and A is a constant which depends on the quark masses and the strength of the interaction. For the s-wave nucleons the ground state ($L = 0$) energies are perturbed only by the Fermi contact term $\vec{S_i} \cdot \vec{S_j} \delta^3(\vec{r_{ij}})$ in (6). In the nucleon rest frame, this perturbation raises the energy of the quark pairs with spin 1 and lowers the energy of pairs with spin 0. It is well known, that this spin dependence is one of the reasons that the $\Delta(1232)$ has a larger mass than the nucleon. In this model it is argued that at large x, where the struck quark carries most of the energy of the nucleon, the spectator quark pair, which is in a lower energy state, has to be in a spin 0 state. This will lead to predictions,

$$A_1^{n,p} \to 1; \qquad \frac{d}{u} \to 0; \qquad \frac{\Delta u}{u} \to 1; \qquad \frac{\Delta d}{d} \to -\frac{1}{3}.$$

Further, the following behavior for the distribution functions are predicted at large x [16],

$$\begin{aligned}
u_v \uparrow (x) &= \left[1 - \frac{1}{2}c_A(x)\right] u_v(x) - \frac{1}{3}\left[1 - c_A(x)\right] d_v(x), \\
u_v \downarrow (x) &= \frac{1}{3}\left[1 - c_A(x)\right] d_v(x) + \frac{1}{2}c_A(x) u_v(x), \\
d_v \uparrow (x) &= \frac{1}{3}\left[1 + \frac{1}{2}c_A(x)\right] d_v(x), \\
d_v \downarrow (x) &= \frac{2}{3}\left[1 - \frac{1}{4}c_A(x)\right] d_v(x).
\end{aligned}$$

With $d(x)/u(x) \simeq \kappa(1-x)$, where $0.5 < \kappa < 0.6$ and $c_A(x) = nx(1-x)^n$, with $2 < n < 4$, one can predict the behavior of A_1 in the valence region. Fig 5 is a compilation of world data for proton and deuteron along with different predictions for A_1. The shaded band given in the figure covers all possible combinations of κ and n.

Duality

In another model [18], different SU(6) breaking scenarios are examined in the context of quark hadron duality, where certain families of resonances are required to die out at large Q^2 in order to maintain duality. In particular three cases are considered, the contributions of families of resonances with either total spin 3/2 ($S = 3/2$), helicity 3/2 ($\sigma_{3/2}$), or symmetric wave functions are required to die out. Since the total photoabsorption cross section $\sigma_{1/2} + \sigma_{3/2}$ is proportional to F_1 and $\sigma_{1/2} - \sigma_{3/2}$ is proportional to g_1, the photoabsorption strengths of transitions from the ground state to each of the final states are incorporated into the model to make predictions for $A_1 \approx g_1/F_1$. For each of these cases the final states are summed by giving an appropriate weight to the absorption strengths and the conditions given above are required to be satisfied as $x \to 1$. The primary idea behind the model is that if a given resonance at $x \sim 1/3$ appears at relatively low Q^2, the $x \sim 1$ behavior of the resonance contribution to the structure function will be determined by the nucleon to resonance transition form factor at large Q^2. The model predicts the following for the above three cases;

1. Spin 3/2 suppression ($S = 1/2$ dominance)
   If the observed Q^2 dependence of the Δ excitation is due to spin dependence, then it is assumed that this is true for all $S = 3/2$ configurations. Which leads to predictions,

$$A_1^{n,p} \to 1; \qquad \frac{d}{u} \to \frac{1}{14}; \qquad \frac{\Delta u}{u} \to 1; \qquad \frac{\Delta d}{d} \to 1,$$

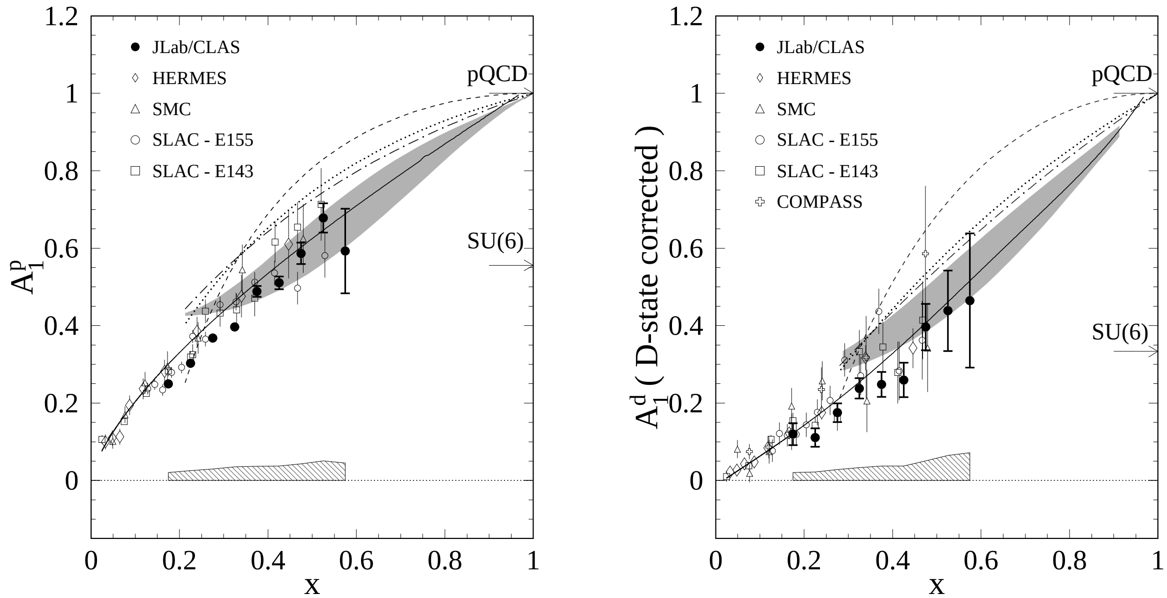

Figure 5: Predictions for A_1^p (left) and A_1^d (right) in the valence region. See the text for an explanation of hyperfine-interactions model (shaded band) and the duality predictions; helicity-1/2 dominance (dashed), spin-1/2 dominance (dotted) and symmetric wave function suppression (dash-dotted). The SU(6) expectation for all x is indicated by the arrow. The solid line is a parameterization of the world data at a fixed $Q^2 = 10$ GeV^2. Also shown are the data from several experiments ([4] - [9], [12], [13], [15].)

2. Helicity 3/2 suppression ($\sigma_{1/2}$ dominance)
   At large x if the virtual photon tends to interact with quarks with the same helicity as the nucleon, the $\sigma_{3/2}$ cross section is expected to be suppressed relative to the $\sigma_{1/2}$ since scattering from a massless quark conserves helicity. Therefore in the limit of $x \to 1$ one has,

$$A_1^{n,p} \to 1; \qquad \frac{d}{u} \to \frac{1}{5}; \qquad \frac{\Delta u}{u} \to 1; \qquad \frac{\Delta d}{d} \to 1,$$

3. Symmetric wave function suppression (Ψ_ρ dominance)
   If the mass difference between the nucleon and the Δ is due to spin dependent forces, then the symmetric part has to be heavier than the antisymmetric part of the wave function. If the symmetric components are suppressed relative to the anti-symmetric components, this will lead to a suppressed d quark distribution relative to the u quark distribution. In the limit $x \to 1$ one has,

$$A_1^{n,p} \to 1; \qquad \frac{d}{u} \to 0; \qquad \frac{\Delta u}{u} \to 1; \qquad \frac{\Delta d}{d} \to -\frac{1}{3}.$$

The resulting ratios for $\Delta u/u$ and $\Delta d/d$ are shown in Fig. 6. The behavior of the ratio $\Delta u/u$ is similar in both the $S = 3/2$ and $\sigma_{3/2}$ suppression models. However the ratio $\Delta d/d$ has a more rapid approach to unity for the $\sigma_{1/2}$ dominance. In the case of symmetric wave

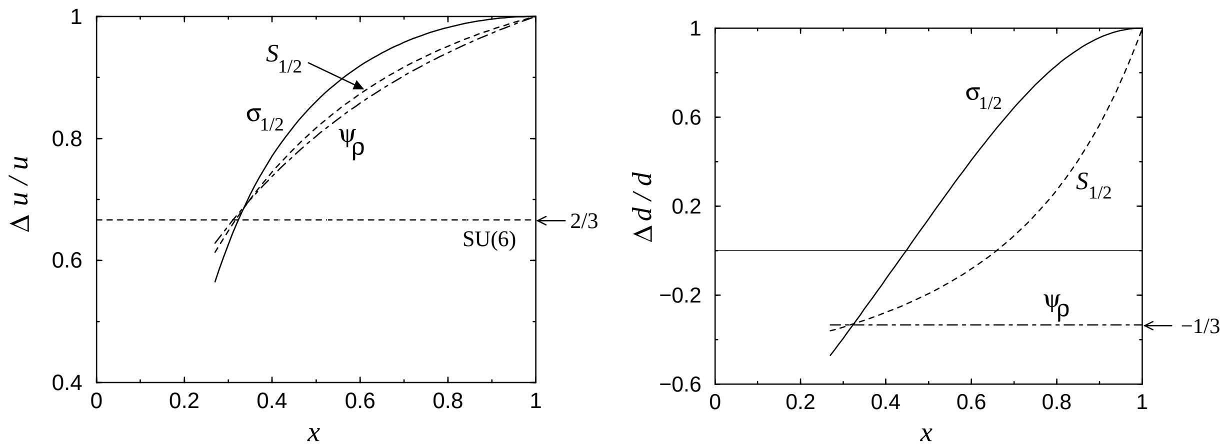

Figure 6: Ratio of $\Delta u/u$ (left) and $\Delta d/d$ (right) in various SU(6) breaking scenarios. Details about all the curves shown are explained in the text.

function suppression, the predicted $\Delta d/d$ ratio shows a very different behavior than in the other two cases.

Model based on one-gluon exchange
In another model [19] one-gluon exchange or pion exchange in QCD are argued to be leading to systematic flavor and spin dependent distortions of the quark distribution functions. This can be related to phenomena such as hyperfine splitting of the baryon and meson mass spectra. Since the quark wave function for the Δ has all diquark configurations with $S = 1$, in the model it is assumed that the one-gluon exchange force induces a higher energy for the $S = 1$ spectator diquark in the nucleon wave function. As $x \to 1$ the model predicts:

$$A_1^{n,p} \to 1; \qquad \frac{d}{u} \to 0; \qquad \frac{\Delta u}{u} \to 1; \qquad \frac{\Delta d}{d} \to -\frac{1}{3}.$$

Perturbative QCD
One of the regions where QCD can be tested at a fundamental level for inclusive lepton-nucleon scattering is the large x domain. In mid 1970's Farrar and Jackson [20] showed that the behavior of the structure functions and hence the quark distributions when x approaches

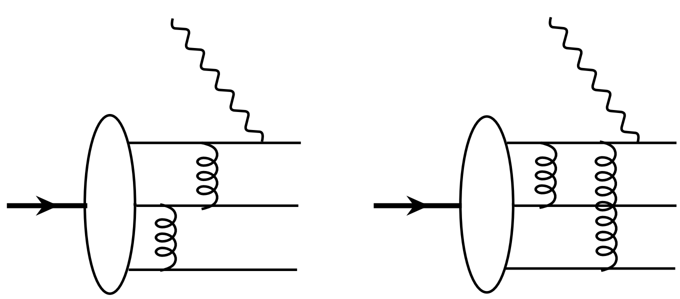

Figure 7: Two diagrams describing the transfer of momenta from the spectator quark pair to the struck quark as $x \to 1$.

1 can be calculated using perturbative QCD methods. In this kinematical regime all of the hadron's light-cone momentum is required to be carried by the struck quark and all the spectator quarks are kinematically forced to be in a $x \sim 0$ state. This represents a very far off-shell configuration of a bound-state wave function. Consequently, predictions for $x \approx 1$ can be made directly from the short-distance properties of QCD. At this kinematic limit, the authors show that the minimal number of gluon exchanges (transverse) required to transfer the momentum of the spectator pair to the struck quark can occur in two ways (Fig 7). There it was argued that, since the angular momentum is conserved, these transverse gluon exchanges can only occur if the spectator quark pair have opposite helicities. Consequently, the struck quark must carry the same helicity as the nucleon (assuming hadron helicity conservation, i.e, if the quark orbital angular momentum is ignored, valence quark helicities sum to the hadron helicity). In this approach, as $x \to 1$, $S_z = 1$ di-quark components are suppressed relative to the $S_z = 0$ di-quark components. This leads to the predictions,

$$A_1^{n,p} \to 1; \qquad \frac{d}{u} \to \frac{1}{5}; \qquad \frac{\Delta u}{u} \to 1; \qquad \frac{\Delta d}{d} \to 1.$$

One important consequence if this picture is experimentally tested to be wrong is that, when the sum of the helicities is not conserved, angular momentum conservation requires either extra constituents or quark orbital angular momentum.

Brodsky, Burkard and Schmidt [21] also obtain a similar result by using counting rules, where the power-law predictions for the large x behavior is given by, $(1-x)^{2n-1+2\Delta S_z}$. Here, n is the minimal number of spectator quark lines, $\Delta S_z = 0$ for quarks polarized parallel and $\Delta S_z = 1$ for quarks polarized anti-parallel to the nucleon helicity. Since $n = 2$ for the valence quark distributions one gets, $(1-x)^3$ and $(1-x)^5$ for the parallel and anti-parallel quark-proton helicities. Therefore, the anti-parallel helicity quark is suppressed by a relative factor $(1-x)^2$, which leads to the same predictions as in the leading order pQCD.

2.1.2 Next to leading order QCD analysis of data

In addition to understanding the $x \to 1$ behavior of the nucleon, spin structure function data taken with the 11 GeV beam energy will be useful in mapping out the x, Q^2 dependence of the polarized parton distributions (PPD) in a kinematic regime where data are scarce.

Leading order (LO) and next-to-leading order (NLO) analyses of polarized deep inelastic scattering data have been performed by many groups such as GRSV [22], LSS [23], BB [24] and AAC [25]. The basic QCD functional form of the spin structure function g_1^p in NLO is approximately given by,

$$g_1^p(x,Q^2)_{pQCD} = \frac{1}{2}\sum e_q^2 \left[(\Delta q + \Delta\overline{q}) \bigotimes \left(1 + \frac{\alpha_s(Q^2)}{2\pi}\delta C_q\right) + \frac{\alpha_s(Q^2)}{2\pi}\Delta G \bigotimes \frac{\delta C_G}{N_f}\right]. \qquad (7)$$

The distributions Δq, $\Delta\overline{q}$ and ΔG evolve in Q^2 according to the spin dependent NLO DGLAP [26] equations. The terms δC_q and δC_g are Wilson coefficients. Beyond LO, Wilson coefficients and parton densities become dependent on the renormalization scheme employed. In the NLO technique parton densities are described using several free parameters and a fit to data is performed to determine each parameter. Fig. 8 is a comparison of parton distributions extracted by different groups.

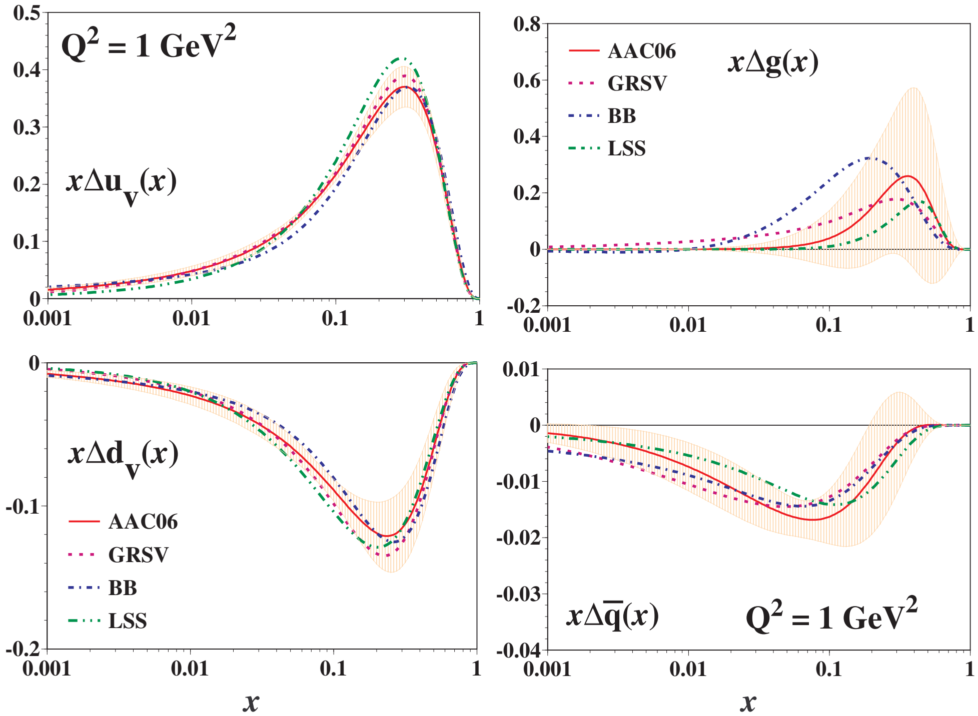

Figure 8: Comparison of polarized parton distributions extracted by different groups. The shaded band is the uncertainties of the AAC06 parameterization [1].

In addition to the logarithmic scaling violations described in the NLO equation given above, higher twist (HT) effects must be taken into account at low Q^2. In the kinematic

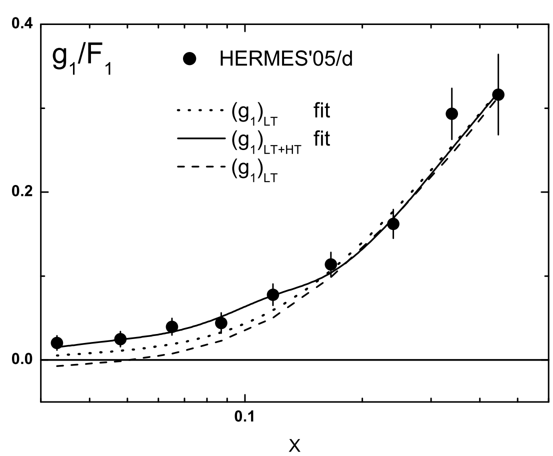

Figure 9: Comparison of fit to the world deuteron data for the ratio g_1/F_1 [23] using only the LT term (dotted) and the HT terms (solid). The dashed curve is the LT term when the HT corrections are taken into account. Also shown are the HERMES deuteron data taken at $Q^2 \approx 1.2 - 2.5$ GeV^2.

regime where HT effects are important, the spin structure function g_1 can be written as,

$$g_1(x, Q^2) = g_1(x, Q^2)_{LT} + g_1(x, Q^2)_{HT},$$

where,

$$g_1(x, Q^2)_{LT} = g_1(x, Q^2)_{pQCD} + h^{TMC}(x, Q^2)/Q^2 + \mathcal{O}(M^4/Q^4),$$

and

$$g_1(x, Q^2)_{HT} = h(x, Q^2)/Q^2 + \mathcal{O}(\Lambda^4/Q^4).$$

Here h^{TMC} is a calculable kinematic correction known as the "target mass correction". The term h denotes the dynamical higher twist corrections to g_1, which represents multi-parton correlations in the nucleon, and cannot be calculated in a model independent way. In the absence of calculations, these HT effects can be determined using data as explained by Leader, Sidorov and Stamenov (LSS) [23]. The proposed measurements will allow extraction of higher twists precisely in the moderate to large x domain. Fig. 9 shows the importance of including HT terms in the determination of the polarized parton distribution functions.

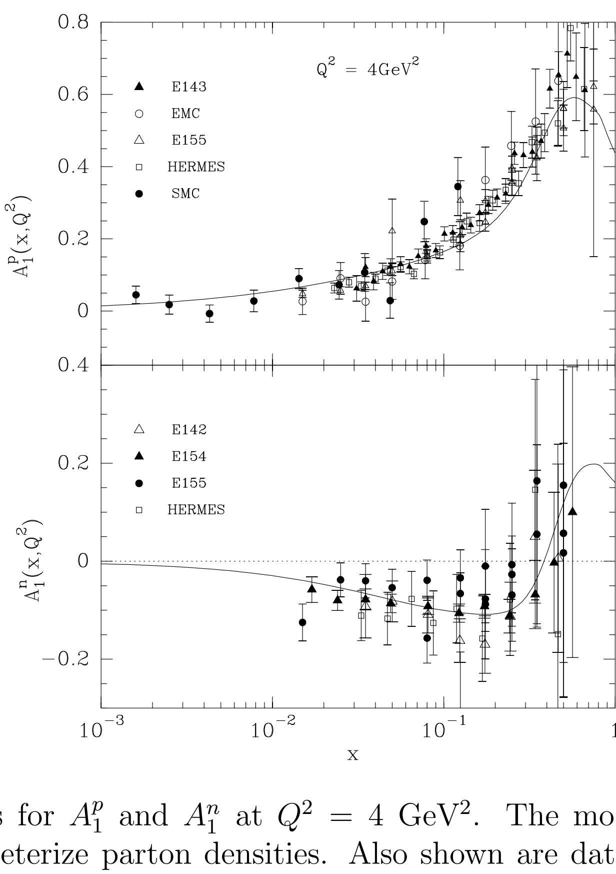

Figure 10: Predictions for A_1^p and A_1^n at $Q^2 = 4$ GeV^2. The model [27] uses a statistical approach to parameterize parton densities. Also shown are data from several different experiments.

In an attempt to reduce the total number of free parameters used in NLO fits, Bourrely, Soffer and Buccella [27] have adopted a statistical framework to construct polarized parton distributions. In this approach, the nucleon is viewed as a gas of massless quarks, antiquarks and gluons in equilibrium at a given temperature in a finite size volume. The parton distributions, $P(x)$, at an input energy scale Q_0^2 are parameterized using the functional form,

$$P(x) \propto \frac{1}{e^{(x-x_{0p})/\overline{x}} \pm 1},$$

where x_{0p} is a constant which can be viewed as the thermo-dynamical potential of the parton p and $\overline{x}$ is the universal temperature. The plus sign corresponds to a Fermi-Dirac distribution for quarks and antiquarks and the minus sign corresponds to a Bose-Einstein distribution for gluons. After constraining the parameterization using known or observed behavior of polarized and unpolarized distributions, a total of 8 parameters are used to fit the existing polarized and unpolarized DIS data. Fig. 10 shows the predicted x dependence of $A_1^{p,n}$.

As described above the extraction of gluon distributions is part of the NLO analysis of data. In addition to lepton-nucleon scattering measurements that can be used to extract the gluon polarization there is a large experimental program at RHIC (Relativistic Heavy Ion Collider) that has begun to produce new measurements on the gluon polarization. However as shown in Fig. 8, even after including those results the gluon polarization at large x is virtually unknown. Therefore it is important to point out the impact the proposed measurements are going to have on the x dependence of the gluon distributions. In particular, the Q^2-dependence of deuteron data at moderate x have been shown to be rather sensitive to the polarized gluon strength in that kinematic region.

2.1.3 Existing data

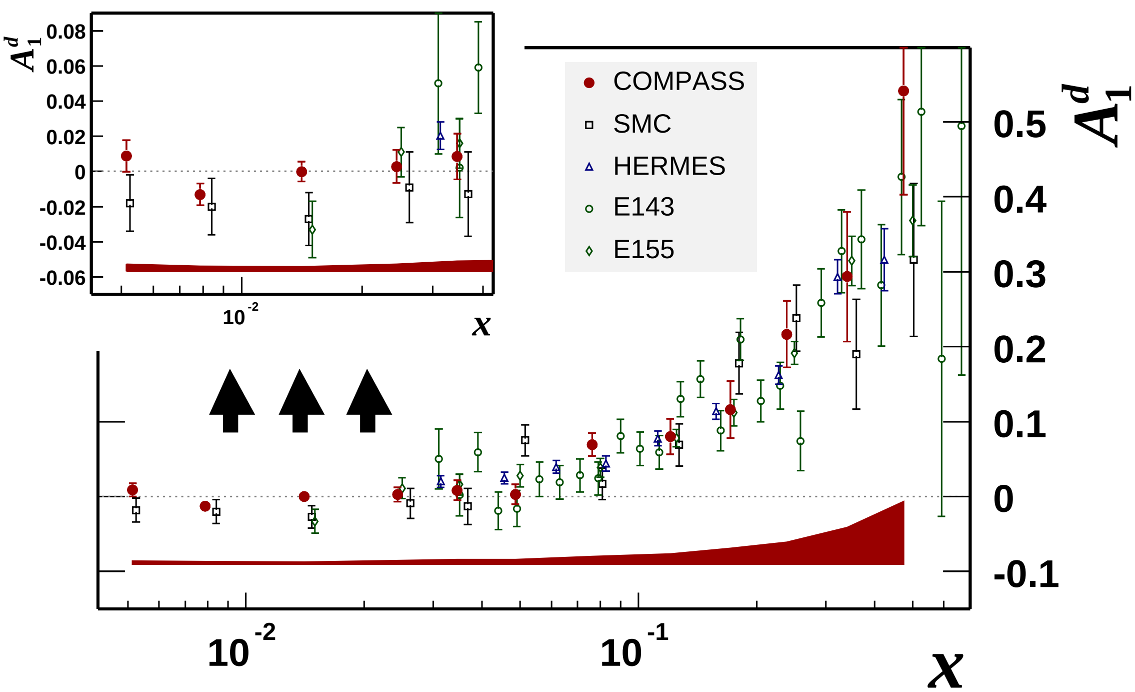

Figure 11: Measurement of the asymmetry A_1^d for the deuteron [13].

During the last two decades many experiments dedicated to measuring the asymmetry A_1 have been conducted at JLab, SLAC, CERN and DESY ([4] - [9], [12], [13], [15].). Most of these experiments cover the large Q^2, small x region (Fig. 11) while 6 GeV beam at JLAB allows us to explore most of the resonance region at low Q^2 values and the DIS region approximately up to $x = 0.6$. Figure 5 is a compilation of existing world data at higher x. Although great experimental effort has been put into measuring the full kinematic regime, counting rates in the large Q^2 large x region accessible at most high energy facilities are very small leading to large statistical uncertainties in spin structure function measurements. The shaded bands in Fig. 12 show the uncertainties in A_1 at $Q^2 = 5$ GeV^2 for the proton and deuteron calculated using most recent DIS data in the AAC06 parametrization. It is obvious from the figure that the large x region is relatively unknown. Whether the $x \to 1$ behavior of nucleon spin structure functions follows any of the predictions described above can be studied experimentally only at Jefferson Lab with the 11 GeV beam. No other accelerators will have the required luminosity and beam energy in the foreseeable future. The data to be collected with the proposed experiment will allow definitive tests of the properties of the valence structure of the nucleon at large x.

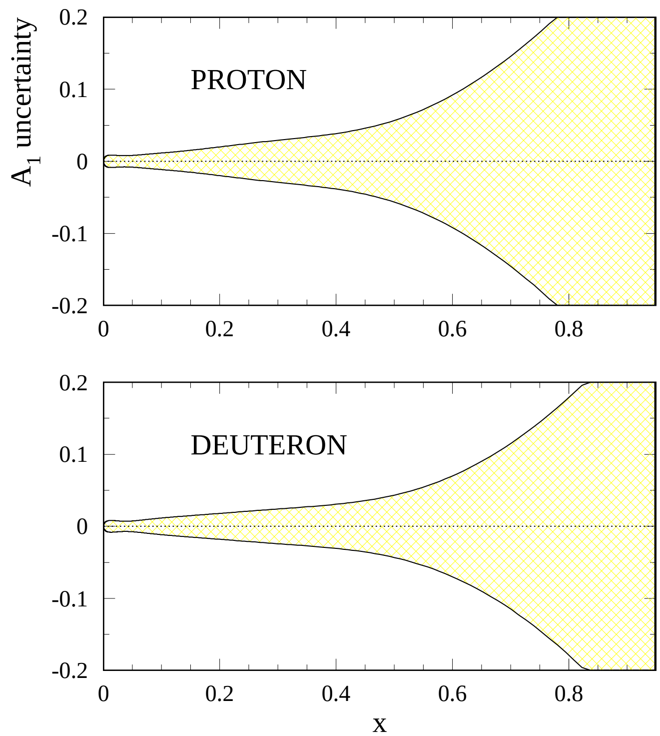

Figure 12: Uncertainties for A_1 at $Q^2 = 5$ GeV^2 calculated in the AAC06 parameterization [1].

2.2 Flavor Decomposition of the Proton Helicity Structure

2.2.1 Introduction

In addition to fully inclusive DIS data, the large acceptance of CLAS12 will allow us to collect data on semi-inclusive (SIDIS) reactions simultaneously. In these reactions, a second particle, typically a meson, is detected along with the scattered lepton. By making use of the additional information given by the identification of this meson, one can learn more about the polarized partons inside the nucleon than from DIS alone. The asymmetry measured by DIS experiments is sensitive to combinations of quark and anti-quark polarized parton distribution functions ($\Delta q + \Delta\bar{q}$), as well as (via NLO analyses) the gluon PDF ΔG. SIDIS experiments exploit the statistical correlation between the flavor of the struck quark and the type of hadron produced to extract information on quark and antiquark PDFs of all flavors separately. Combined NLO analyses of DIS and SIDIS data can therefore give a more detailed picture of the contribution of all quark flavors and both valence and sea quarks to the total nucleon helicity.

Beyond the determination of the polarized PDFs, SIDIS data can also yield a plethora of new insights into the internal structure of the nucleon as well as the dynamics of quark fragmentation. For instance, looking at the z- and p_T-dependence of the various meson asymmetries (both double spin asymmetries and single spin target or beam asymmetries), one can learn about the intrinsic transverse momentum of quarks and their orbital angular momentum. Another topic of high interest concerns higher twist contributions to the nucleon structure, such as quark-quark and quark-gluon correlations. A full discussion of the possibilities opened up by high precision SIDIS data (finely binned in x, Q^2, z and p_T) is beyond the scope of the present proposal. Here, we concentrate only on the extraction of polarized quark distributions Δq and $\Delta\bar{q}$. A companion proposal for the case of unpolarized targets is being submitted to this PAC. A future comprehensive proposal including all polarization degrees of freedom is under preparation and is outlined in a Letter of Intent to PAC30 [28]. For now we just want to point out that the experiment proposed here will "automatically" collect all the necessary data, at least for longitudinally polarized targets, with unprecedented precision.

2.2.2 Models and Techniques

One of the original descriptions of SIDIS observables in double polarization measurements was given by Frankfurt, et. al. [29] within the framework of the standard parton model of Feynman. In this approach, the number of hadrons (N^h) produced in an SIDIS experiment may be expressed in terms of quark distributions $q(x)$ and fragmentation functions $D(z)$ where x is the Bjorken variable and $z \equiv E_h/\nu$ represents the energy fraction carried by the resulting hadron (h). (The dependence on p_T has been integrated over.) In the case that the incident lepton and target are longitudinally polarized, the number of hadrons produced may be expressed as

$$N^h_{\uparrow\downarrow} \propto \sum_q e_q^2 q_{\Uparrow}(x) D_q^h(z) \tag{8}$$

where $\uparrow$ and $\downarrow$ represent the orientation of the incident lepton and target nucleon respectively, while $\Uparrow$ is the spin of the quark with respect to the nucleon spin. The sum is over all quark and anti-quark flavors q. The fragmentation function is assumed to be independent of the quark helicity ($D_{q_\Uparrow} = D_{q_\Downarrow} \equiv D_q$) since the fragmentation process conserves parity and the hadron polarization is not observed. Using helicity independent fragmentation as well as the application of isospin and charge conjugation symmetry, one may define a set of "favored" fragmentation functions

$$D_1(z) = D_u^{\pi+}(z) = D_d^{\pi-}(z) = D_{\bar{d}}^{\pi+}(z) = D_{\bar{u}}^{\pi-}(z) \tag{9}$$

for the case that a charged pion is observed. The term "favored" labels the fragmentation functions for the quarks which are contained in the hadrons isospin wavefunction. Similarly, the "unfavored" fragmentation function would be denoted as

$$D_2(z) = D_d^{\pi+}(z) = D_u^{\pi-}(z) = D_{\bar{u}}^{\pi+}(z) = D_{\bar{d}}^{\pi-}(z). \tag{10}$$

In principle, the fragmentation functions D_1 and D_2 can be measured in unpolarized SIDIS experiments as well as in e^+e^- collider experiments. Once they are known, one can use them to extract information on the quark flavor contribution to a given SIDIS reaction (see below). However, one can also find particular combinations of measurements that will directly yield information on the underlying quark polarizations (at least in leading order), without requiring knowledge of D_1 and D_2.

One such quantity is the SIDIS pion asymmetry [29]

$$A^{\pi^+-\pi^-} = \frac{N_{\uparrow\downarrow}^{\pi+} - N_{\uparrow\downarrow}^{\pi-} - N_{\uparrow\uparrow}^{\pi+} + N_{\uparrow\uparrow}^{\pi-}}{N_{\uparrow\downarrow}^{\pi+} - N_{\uparrow\downarrow}^{\pi-} + N_{\uparrow\uparrow}^{\pi+} - N_{\uparrow\uparrow}^{\pi-}}. \tag{11}$$

This asymmetry can be measured on the proton and the deuteron and only depends on the valence quark distributions u_V, Δu_V, d_V and Δd_V:

$$A_p^{\pi^+-\pi^-}(x) = \frac{4\Delta u_V(x) - \Delta d_V(x)}{4u_V(x) - d_V(x)} \qquad A_d^{\pi^+-\pi^-}(x) = \frac{\Delta u_V(x) + \Delta d_V(x)}{u_V(x) + d_V(x)}, \tag{12}$$

at least in a kinematic region where one is not completely dominated by sea quarks. It should be noted that the fragmentation functions cancel in the definition of the asymmetry above. (However, there could be a problem if D_1 and D_2 are similar in size, because both the numerator and denominator become very small in that case). Using the above system of equations and measurements of the unpolarized distribution functions $u_V(x)$ and $d_V(x)$, one can extract the polarized valence quark distribution functions $\Delta u_V(x)$ and $\Delta d_V(x)$ from SIDIS asymmetry measurements.

The more straightforward approach of extracting polarized PDFs from SIDIS measurements by utilizing previous knowledge of the fragmentation functions D_1 and D_2 was applied first by the Spin Muon Collaboration (SMC) [30]. They extracted Δq (in LO) using a system of equations involving both the DIS and SIDIS measurements. The system of equations is formulated using Eq. 5 for the DIS measurements and expressing the SIDIS asymmetries as

$$A_1^h(x, Q^2, z) = \frac{\sum_q e_q^2 \Delta q(x, Q^2) D_q^h(z, Q^2)}{\sum_{q'} e_{q'}^2 q'(x, Q^2) D_{q'}^h(z, Q^2)} \tag{13}$$

using Eq. 8. A system of 6 equations involving A_1^p,A_1^d,$A_{1,p}^{h+}$,$A_{1,p}^{h-}$,$A_{1,d}^{h+}$, and $A_{1,d}^{h-}$ were constructed based on Eq. 5 and 13 in the form

$$\vec{A} = \mathcal{B}\Delta\vec{q} \tag{14}$$

Parameterizations were used for the unpolarized quark distributions and the fragmentation functions.

The HERMES Collaboration has extracted LO polarized quark distribution functions from SIDIS measurements [31] using a similar method commonly referred to as the "Purity" method (basically an extension of the SMC approach above). The Purity $\mathcal{P}_q^h(x, Q^2, z)$ represents the probability that the observed final state hadron h originated from a quark of flavor q and is defined in terms of the unpolarized quark distributions such that

$$\mathcal{P}_q^h(x, Q^2, z) = \frac{e_q^2 q(x, Q^2) D_q^h(z, Q^2)}{\sum_{q'} e_{q'}^2 q'(x, Q^2) D_{q'}^h(z, Q^2)}. \tag{15}$$

The underlying assumption is that the hard scattering process and fragmentation may be factorized. Substituting this definition into Eq. 13 leads to

$$A_1^h(x, Q^2, z) = \sum_q \mathcal{P}_q^h(x, Q^2, z) \frac{\Delta q(x, Q^2)}{q(x, Q^2)} \tag{16}$$

A fitting procedure is again implemented which uses minimization methods to solve the vector equation equivalent of Eq. 16 :

$$\vec{A} = \mathcal{P}\vec{Q} \tag{17}$$

where $\vec{A}$ contains both inclusive and semi-inclusive asymmetry measurements on both proton and deuteron targets and $\vec{Q}$ represent the ratio of polarized to unpolarized quark distribution functions. The Purity method relies on the LUND model's [32] ability to describe the quark fragmentation process. In practice, the HERMES collaboration determines $\mathcal{P}$ using a LUND based Monte Carlo simulation tuned to reproduce the hadron multiplicities observed by the HERMES experiment.

The methods of extracting $\Delta q(x)$ employed by the SMC and HERMES experiments rely on the assumption that at LO the cross-sections factorize into quark distributions which depend only on x and fragmentation functions which depend on z as in Eq. 8. Indeed, factorization appears to work for $z \geq 0.2$ and $0.02 \leq x \leq 0.3$, based on the lack of any z dependence in the extraction of the ratio $\frac{\bar{d}-\bar{u}}{u-d}$ from SIDIS pion production [33]. A more stringent test of fragmentation was proposed in Reference [34] in which the proton-neutron difference asymmetry ($\Delta R_{np}^{\pi^+ + \pi^-}$) is compared to an expression involving the DIS structure functions g_1 and F_1:

$$\begin{aligned} \Delta R_{np}^{\pi^+ + \pi^-}(x, Q^2, z) \equiv & \frac{\Delta\tilde{\sigma}_p^{\pi^+ + \pi^-} - \Delta\tilde{\sigma}_n^{\pi^+ + \pi^-}}{\tilde{\sigma}_p^{\pi^+ + \pi^-} - \tilde{\sigma}_n^{\pi^+ + \pi^-}}(x, Q^2, z) \\ = & \frac{g_1^p - g_1^n}{F_1^p - F_1^n}(x, Q^2). \end{aligned} \tag{18}$$

From the existing EG1 experiment with CLAS at 5.7 GeV beam energy, we can already infer that factorization is not badly broken, even at these rather low energies. As shown in Fig. 13, our data on the asymmetries for all 3 charge states of the pion agree well with PEPSI [32] Lund Monte Carlo calculations "tuned" to the data taken by HERMES at much

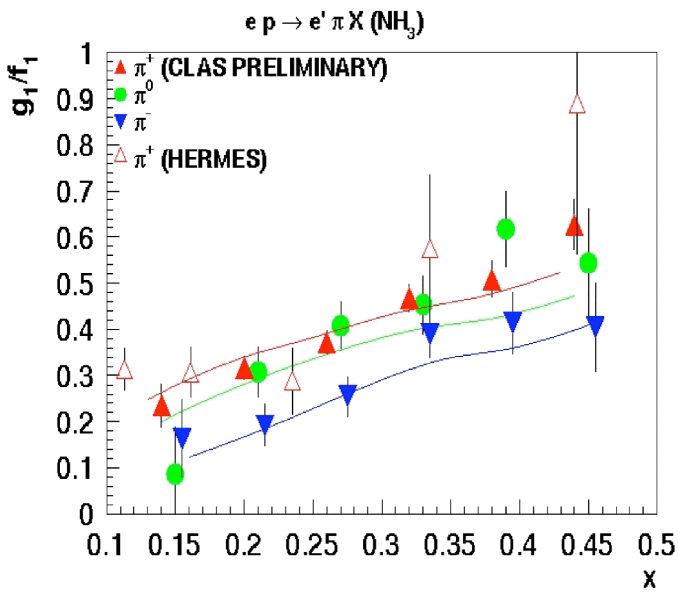

Figure 13: Comparison of various SIDIS asymmetries measured with 5.7 GeV beam in CLAS with predictions from hadronization models and higher energy data.

higher Q^2. We also see only weak p_T and z-dependence in the range $0.3 \leq z \leq 0.7$, and our inclusive data agree well with the asymmetries for the π^0 alone or the sum of π^+ and π^-. Clearly, factorization should work even better in the kinematics of the proposed experiment. We will be able to thoroughly test this assumption.

For a more accurate extraction of polarized PDFs, one has to go beyond leading order and treat DIS and SIDIS data consistently up to NLO. The extraction of Δq at NLO based on Eq. 12 has been proposed by Christova and Leader [35]:

$$\begin{aligned}
A_{1p}^{\pi^+-\pi^-} &= \frac{(4\Delta u_v - \Delta d_v)\,[1 + \otimes(\alpha_s/2\pi)\Delta C_{qq}\otimes]\,(D_u^{\pi^+-\pi^-})}{(4u_v - d_v)\,[1 + \otimes(\alpha_s/2\pi)C_{qq}\otimes]\,D_u^{\pi^+-\pi^-}}, \\
A_{1d}^{\pi^+-\pi^-} &= \frac{(\Delta u_v + \Delta d_v)\,[1 + \otimes(\alpha_s/2\pi)\Delta C_{qq}\otimes]\,(D_u^{\pi^+-\pi^-})}{(u_v + d_v)\,[1 + \otimes(\alpha_s/2\pi)C_{qq}\otimes]\,(D_u^{\pi^+-\pi^-}}.
\end{aligned} \tag{19}$$

The term $\otimes(\alpha_s/2\pi)\Delta C_{qq}\otimes$ represents a double convolution of the form $\Delta q \otimes \Delta C \otimes D$ where C is a Wilson coefficient as derived in Reference [36]. The unpolarized analog of the double convolution, $q \otimes C \otimes D$, is derived in Reference [37]. The function $D_u^{\pi^+-\pi^-}$ may be measured using unpolarized semi-inclusive pion production with NLO corrections similar to Eq. 19. The difference asymmetries in Eq. 11 may be cast in terms of the usual charged hadron asymmetries

$$A^h = \frac{N^h_{\uparrow\downarrow} - N^h_{\uparrow\uparrow}}{N^h_{\uparrow\downarrow} + N^h_{\uparrow\uparrow}} \tag{20}$$

weighted by the ratio of the charge conjugate hadron rates such that in the case of pion production Eq. 11 becomes

$$A^{\pi^+-\pi^-}(x) = \frac{R}{R-1}A^{\pi^+}(x) - \frac{1}{R-1}A^{\pi^-}(x) \tag{21}$$

where $R \equiv \frac{N^{\pi^+}}{N^{\pi^-}}$.

We are presently studying the impact our data would have on such a combined NLO analysis.

2.2.3 Existing Data

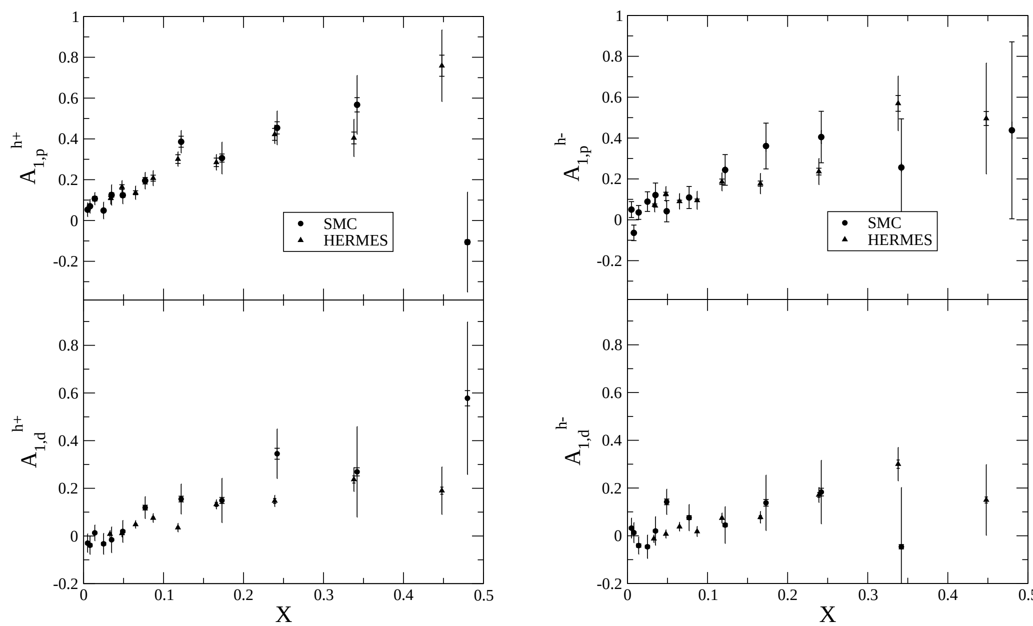

Figure 14: SIDIS results from the SMC and Hermes experiments. The left graph represents the measured asymmetry A_1 of positive hadrons using a proton target $A_{1,p}^{h+}$ and deuteron target $A_{1,d}^{h+}$ as a function of x. The results for negative hadrons are also shown in the right hand side graph.

The SMC experiment at CERN [30] measured DIS and SIDIS asymmetries using polarized muons as the probe and polarized ammonia or deuterated butanol as the proton and deuteron target, respectively. This experiment has been followed by the COMPASS experiment at CERN [38] which is now collecting data. The HERMES collaboration at DESY [31] uses polarized electron and positron beams stored in the HERA electron proton collider and an internal polarized gas target. HERMES will continue to take data until 2007 (but not on longitudinally polarized nucleon targets). Figures 14 and 15 show the level of consistency between the SMC and HERMES SIDIS experiments. The present data set in Figure 15 has yet to reach a region of x >0.5 where pQCD predicts that $\frac{\Delta d}{d}$ should become positive and begin approaching unity as $x \to 1$.

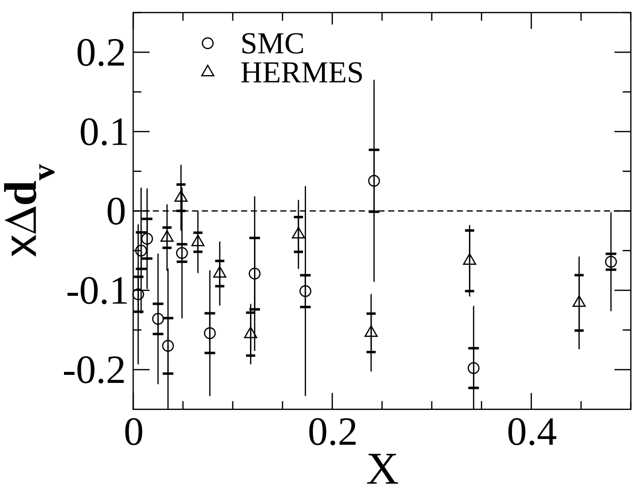

Figure 15: SIDIS results from the SMC and Hermes experiments. This graph illustrates the extracted value of the polarized down quark distribution.

Our present knowledge of polarized sea quark distributions from these experiment is also rather limited. HERMES results on Δs are consistent with zero for the x-region covered, while DIS data seem to indicate a negative contribution of the strange sea to the nucleon spin. Another example is the difference between anti-up and anti-down polarized quark distribution, shown in Fig. 16. This quantity is of high interest since the corresponding unpolarized quark distributions are known to show substantial differences. However, the uncertainties in the existing data are too large to draw definite conclusions.

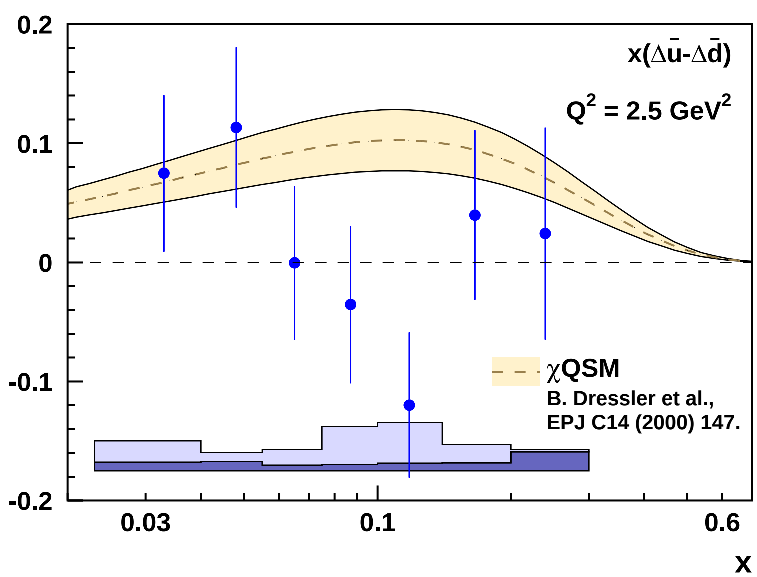

Figure 16: SIDIS results from the Hermes experiments for the difference between the polarized anti-u and anti-d quark distributions.

The goal of our proposed experiment is to gather a vastly larger data set on SIDIS in the region $0.1 \leq x \leq 0.8$. At large x, these data will confirm the behavior of the valence quarks (without sea quark contamination) and test the convergence of Δu_V and Δd_V towards $x \to 1$. A consistent NLO analysis of both our DIS and SIDIS data, together with the remaining world data, will ultimately lead to the most reliable separation of valence and sea quark contributions of each quark flavor to the nucleon helicity structure in the region $0.1 \leq x \leq 0.8$. With the present configuration of CLAS12, kaons can only be separated from pions below a momentum of 4.5 GeV/c and will yield only limited additional constraints, especially on the strange and non-strange sea. This contribution could be expanded significantly if CLAS12 can be upgraded with additional particle ID capacity at a later time.

2.3 Sum Rules, Higher Twist and Duality

Moments of structure functions provide powerful insight into the underlying structure of nucleons. Recent inclusive data at Jefferson Lab have enabled us to evaluate some of these moments at low and intermediate Q^2 [10, 11, 39]. A primary goal was to study the transition from partonic to hadronic degrees of freedom. With a maximum beam energy of 6 GeV, however, the measured strength of the moments becomes rather limited for Q^2 greater than a few GeV^2. See for example Fig. 17 which displays the fraction of moment Γ_1^p measured with the present CLAS detector (dotted blue line) compared to the full moment (black line). The 12 GeV upgrade will allow us to address this problem and push the measurement to higher Q^2. Fig. 17 gives the measured strength of the integral with CLAS12 and a 11 GeV beam (red dashed line). The corresponding kinematic coverage is given in Fig. 18 (dark blue area).

2.3.1 Scientific motivations for studying moments

At large Q^2 the fundamental Bjorken Sum Rule relates the difference of the first moment of the spin structure function g_1 for the proton and the neutron to the axial coupling constant [40]. At the other end of the spectrum, $Q^2 = 0$, the Gerasimov-Drell-Hearn (GDH) Sum Rule links the difference of spin dependent cross sections, integrated over ν, to the anomalous magnetic moment of the nucleon [41]. These two sum rules are aspects of a more general sum rule derived by Ji and Osborne [42].

$$4\int_{\nu_0}^{\infty} G_{1(2)} \frac{d\nu}{v} = \overline{S_{1(2)}} \tag{22}$$

where ν is the energy transfer, ν_0 is the inelastic threshold, G_1 and G_2 are nucleon spin structure functions ($g_1 = M\nu G_1$ and $g_2 = \nu^2 G_2$) and $\overline{S_{1(2)}}$ are the spin-dependent Compton amplitudes with the elastic contribution excluded. At low Q^2, the first moment of g_1 is constrained by the GDH sum rule and is an excellent testing ground for chiral perturbation theory calculations, while at large Q^2 it can be compared to operator product expansion (OPE) calculations. At moderate Q^2, lattice QCD calculations can produce results for higher twist terms, thus extending the domain of applicability of OPE. However, when going to low Q^2, due to the increasing uncertainty on the strong coupling constant and on the convergence of the higher twist series, the OPE formalism becomes unusable. To bridge this final gap, lattice QCD can be used to compute spin-dependent Compton amplitudes at any Q^2. Hence, having a relation such as Eq. 22 valid at any Q^2 provides us with a quantity, the

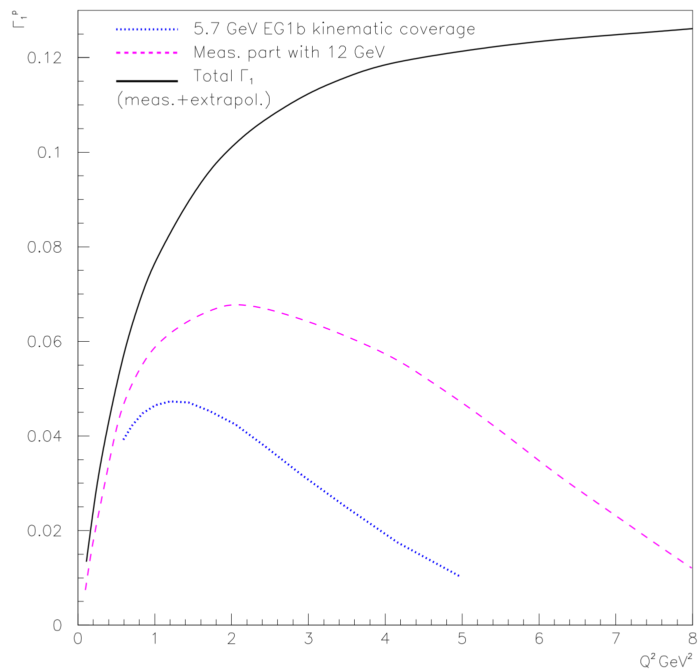

Figure 17: The first moment of the g_1^p spin structure function, Γ_1^p. The continuous black line is an estimate of Γ_1^p based on the Bianchi and Thomas parameterization [54]. The dashed pink line represents the measurable part of Γ_1^p using CLAS12 and a beam energy of 11 GeV. The dotted blue line is the portion of Γ_1^p measured with CLAS and a 5.7 GeV beam energy (kinematic coverage of the EG1b experiment).

GDH sum, that can be computed and compared to experiment at any Q^2. This offers an unique opportunity to study the parton-hadron transition.

Higher moments are also of interest: generalized spin polarizabilities, γ_0 and δ_{LT}, are linked to higher moments of spin structure functions by sum rules based on similar grounds as the GDH sum rule. Higher moments are less sensitive to the unmeasured low-x part since they are more weighted at high-x. As a consequence, they can be better measured at moderate Q^2 and measurements are possible up to higher Q^2 compared to first moments, see Fig. 19. Just like the GDH/Bjorken sum rules, measurements of the Q^2-evolution allow us to study the parton-hadron transition since theoretical predictions exist at low and large Q^2 [39]. In addition, spin polarizabilities are also fundamental observables characterizing the nucleon structure and the only practical way presently known to measure generalized spin polarizabilities is through measurement of moments and application of the corresponding sum rules.

Finally, moments in the low ($\simeq 0.5$ GeV^2) to moderate ($\simeq$4 GeV^2) Q^2-range enable us to extract higher twist parameters. Those are sensitive to correlations between quarks in the nucleon. This extraction can be done by studying the Q^2 evolution of first moments [39]. Measurements of higher twists have been consistently found to have, overall, a surprisingly

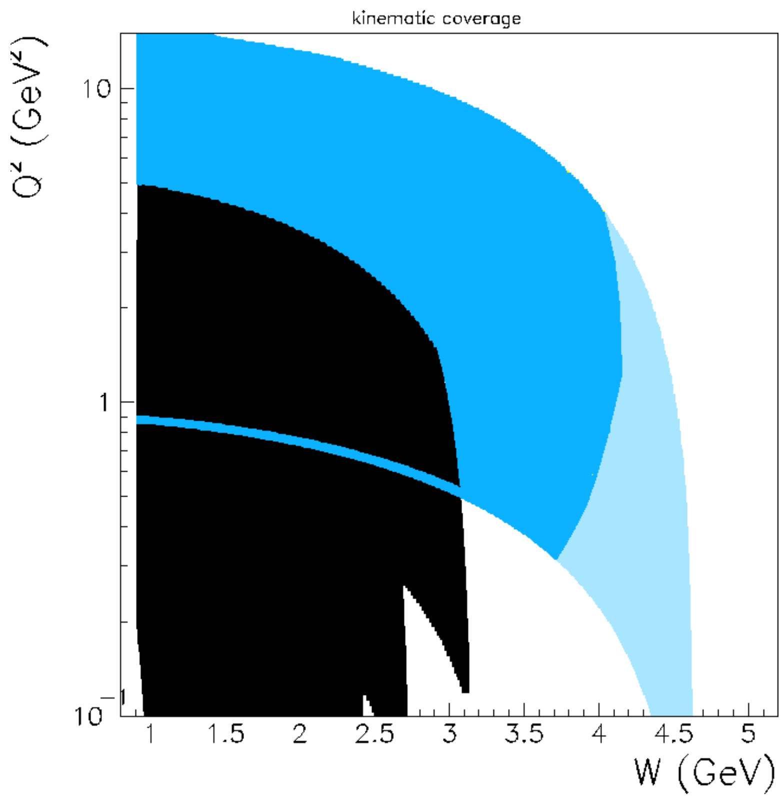

Figure 18: Kinematic coverage of CLAS12 with a 11 GeV beam. The dark blue area is for data taking limited to kinematics for which the proton inelastic cross-section is larger than the proton elastic tail. This high-w (or low-x) limit may be extended, for example by requiring the detection of an hadron in addition to the electron (light blue area). Here, however, we will assume conservatively that the integration of the moment is limited by the elastic tail (darker area). The black area is the kinematic coverage of the CLAS EG1 and EG4 experiments.

smaller effect than expected. This seems to be due in part to cancellation occurring in the twist series [39]. Going to lower Q^2 enhances the higher twist effects but makes it harder to disentangle a high twist from the yet higher ones. Furthermore, in the specific case of extracting higher twists using moments, the uncertainty on α_s becomes prohibitive at low Q^2. Hence, higher twists turn out to be hard to measure, even at the present JLab energies. Measuring higher twists at higher Q^2 removes the issues of disentangling higher twists from each others and of the α_s uncertainty. The smallness of higher twists, however, requires a statistically precise measurements with small point to point correlated systematic uncertainties. Such precision at moderate Q^2 has not been achieved by the experiments done at high energy accelerators, while JLab at 12 GeV presents the opportunity to reach it. In particular, by extending the fraction of the moments measured by a single experiment with high precision (see Fig. 17), we can reduce systematic and statistical errors on the extrapolation to $x = 0$ which has to be done to compute the moments.

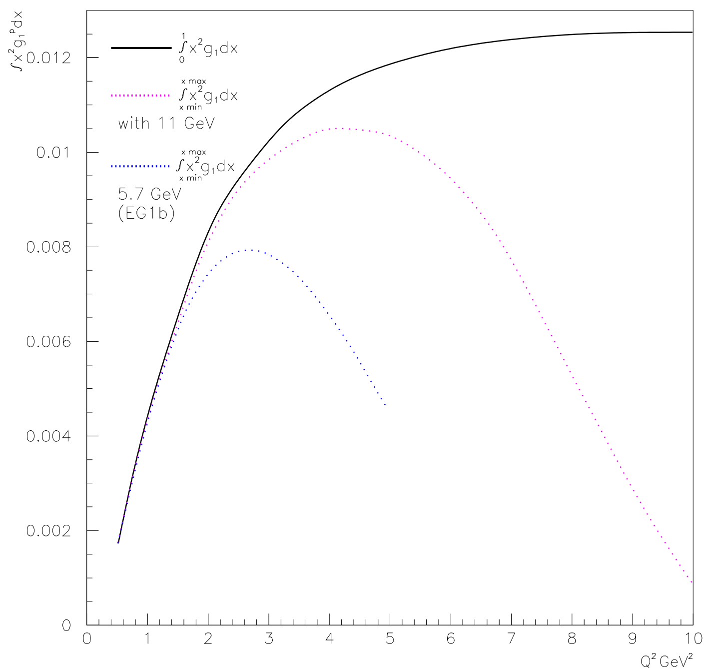

Figure 19: Second Moment of g_1^p. The notations and procedure are the same as for Fig. 17

3 Experimental Details

3.1 CLAS12

The proposed experiment will use the upgraded CLAS12 spectrometer in its standard configuration. We will run at the maximum magnetic field with inbending polarity. The central tracker will also be used for coincident detection of protons and pions. The solenoid for the central tracker serves simultaneously to provide the magnetic field for the polarized target. Additional details on CLAS12 can be found in the document provided as an appendix to all CLAS12 proposals.

3.2 Polarized Target

The proposed experiment requires use of a polarized solid state target. The target will be polarized via the method of Dynamic Nuclear Polarization (DNP) which is a well established technique that has been used extensively in nuclear and particle physics experiments, including the ones performed in Hall B of Jefferson Lab. Dynamically polarized target systems consist of a hydrogenated (polarized protons) or deuterated (polarized neutrons) compound containing paramagnetic centers, such as unpaired electrons, placed in a high magnetic field and cooled to low temperatures, with a B/T ratio of the order of 5 Tesla/Kelvin. In these conditions, the free electron spins can approach polarization of 100%. The high polarization of unpaired electrons is then transferred dynamically to the nucleons by irradiating the target material at frequency near that of electron spin resonance. This technique typically achieves a proton polarization of 80-90%, and a deuteron polarization of 30-40%. The nucleons in the target will be polarized either parallel or anti-parallel to the electron beam direction.

The main systems required to realize DNP are the superconducting magnet to provide a strong (5 T) field, a ^{4}He evaporation refrigerator to maintain the target material at 1 K, a target insert which will house the target material and some additional instrumentation, a microwave system to transfer the polarization to the nucleon spins and a Nuclear Magnetic Resonance (NMR) system to determine the state of polarization.

In CLAS12 the polarizing magnetic field will be provided by the superconducting solenoid of the central detector. In this configuration, the central detector can be used also for polarized target experiments, yielding wide coverage for measurements of multi-hadron final states. The solenoid magnet is in the design stage, and not all parameters are well known at the moment. Some additional correction coils might be necessary to improve the field uniformity around the target cell. The DNP method requires that the target material is placed in a magnetic field of uniformity $\frac{\Delta B}{B} < 10^{-4}$. The current magnet design provides for such a region of field uniformity in a cylinder of 30 mm in diameter and 100 mm in length. Some properties of the magnet are listed in Table 1.

Type	Superconducting solenoid
Aperture	0.78m warm bore
Central field	2.5-5T
Dimensions	1.10m OD x 0.78m ID x 1.055m long
Region of $\frac{\Delta B}{B} < 10^{-4}$	cylinder: 10 cm long, 3 cm OD

Table 1: CLAS12 solenoid properties

The target cryostat will house the evaporation refrigerator, the target insert and some instrumentation necessary for the microwave and NMR operations. The cryostat needs to be designed to allow its operation in a warm bore magnetic field. A conceptual design of the target cryostat is shown in Fig. 20. The main component of the cryostat is a ^{4}He evaporation refrigerator. The refrigerator is inserted horizontally through a pumping tube between the pumps and the evaporation chamber. One important difference between this design and the previously used polarized target in Hall B is that the refrigerator will be residing along the beam line, so that the amount of materials in the way of the beam needs to be minimized. Liquid helium is supplied to the refrigerator through a transfer line from a dewar located outside of the detector. The liquid enters a copper separator pot, which will have a doughnut-like shape in order not to obstruct the beam path.

In the separator, LHe is separated from the vapor by a sintered filter. The vapor is pumped away cooling the upper heat exchangers, and the liquid is used to cool the target material. There are two needle valves that can transport LHe from the separator pot to the evaporation chamber. The bypass valve allows helium to be transported through a straight tube, going directly to the evaporation chamber, and is used for initial cool down of the target system. The run valve directs helium flow throw a spiral tube, thermally sunk to the copper plated lower hear exchangers. The run valve is typically used during the experiment.

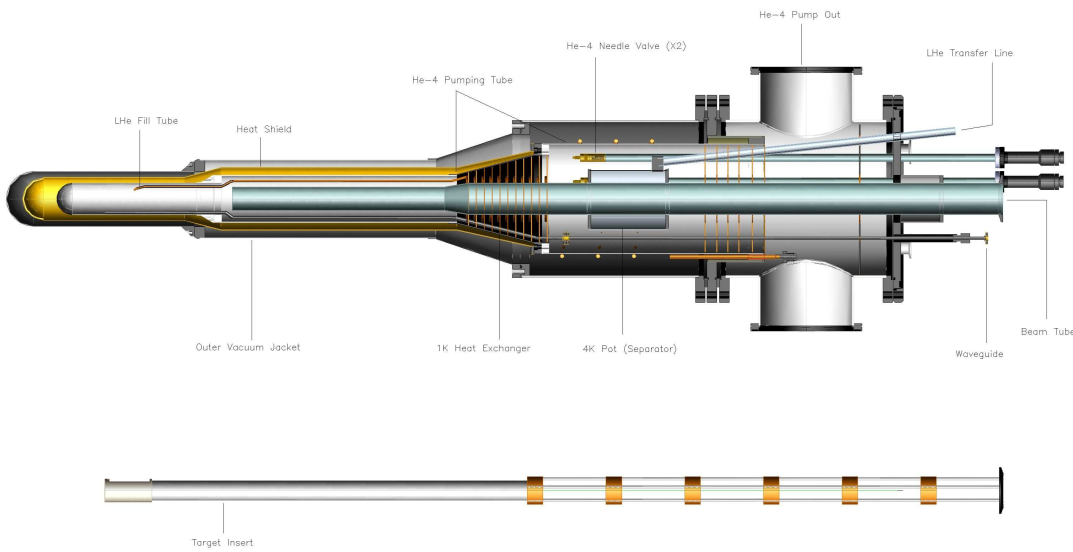

Figure 20: A schematic drawing of the polarized solid target cryostat and target insert for CLAS12.

The evaporation chamber will be situated in the bore of the magnet. The central tracker will also be installed in the magnet bore, surrounding the target, and impose constraints on the chamber dimensions. The minimum outer diameter in the present design of the evaporation chamber is 10 cm. This volume will contain the outer vacuum space, heat shield and the evaporation chamber.

The target material will be placed in the cell inside of a cup, with both containers made of hydrogen free plastic. The cup will be attached to a thin aluminum structure that can be inserted through the beam tube. The schematic of the insert is shown on the bottom of Fig. 20. The dimensions of the target cell will be determined by the size of the region of field uniformity, and geometric constraints of the cryostat. The cup will have an opening on the top for the LHe fill, while the cell will have small holes so that the target material will be sitting in a bath of LHe, while also being showered by LHe coming from the run valve. The flow of LHe in the cryostat will be maintained by a series of pumps located outside of the cryostat. The entrance and exit windows of the target cell and cup could be made out of thin aluminum or Kapton foils. The microwave radiation needed to polarize the target will be guided through a designated waveguide inserted through the upstream entrance window of the cryostat. The guide will have a slit directly underneath the target cup, providing continuous microwave radiation directed at the target cell. With this arrangement, the target cup will act as a resonating cavity.

Name	Material	Dimensions
Outer Vacuum Jacket	Al	0.5 mm
Heat Shield	Al	0.5 mm
Cup Wall	Kel-F	0.5 mm
Cup/Cell Windows	Al	0.025 mm
Cell	Kel-F/torlon	0.3 mm

Table 2: New cryostat and insert design parameters

Ammonia and deuterated ammonia will be used as target material with the electron beam and CLAS12. (We will also investigate the possibility of using ^{6}LiD as a target material.) The ammonia will be frozen and broken up into small beads (to optimize the cooling surface) which fill the target cup. These targets offer high polarization, good resistance to radiation damage, and a relatively high ratio of polarizable nucleons per total number of nucleons. Ammonia can accumulate a charge of $\sim 10^{15}$ electrons/cm^2 before showing signs of deterioration. Accumulated radiation damage can be mostly restored through the annealing process, in which target material is heated to temperatures of 80-90 K for short periods of time [43]. Some parameters of frozen ammonia are listed in Table 3.

Chemical Structure	$NH_3(ND_3)$
Target Diameter	up to 30 mm
Target Length	up to 100 mm
Density	0.917(1.056) g/cm^3
Dilution Factor	$\approx 0.15(0.22)$
Packing Factor	≈ 0.6

Table 3: Some Parameters of the Ammonia Targets

In order to determine the effective dilution factor f_{eff}, it will be necessary to collect data on the unpolarized material. A thin carbon target can be placed downstream in the same target cup for this purpose.

The target polarization will be monitored during the run via the NMR system, in the field of solenoid magnet. The calibration of the proton NMR can be done by measurements of polarization in thermal equilibrium, taken with the polarizing magnet. In cases when the deuteron signal is too small for the thermal equilibrium measurement, the polarization can be monitored through the ratio of the two peaks of the NMR signal (R-ratio method [44]). The target cell size in the current design is relatively large, which will allow for placement of the coils inside of the cell resulting in a measurable thermal equilibrium signal, so the polarization of deuterium will be monitored by the area and ratio methods.

Typical NMR signals for the proton and deuterium targets are shown in Fig. 21 [45]. The signals are obtained from the small target cells with NMR coils wrapped on the ouside, and represent the minimum expected quality.

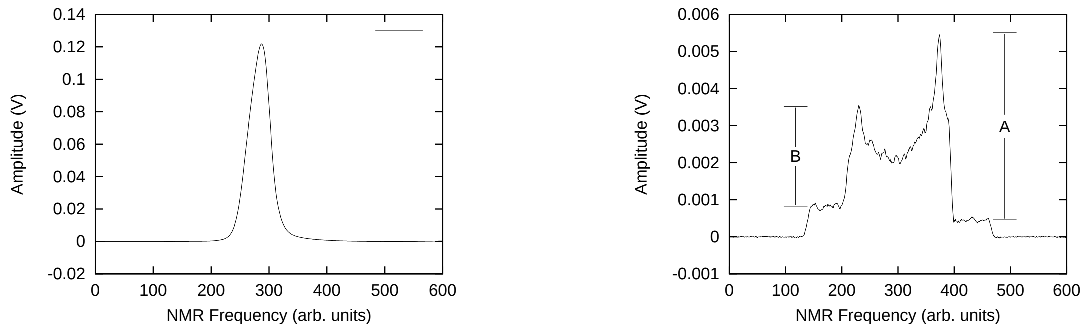

Figure 21: NMR signals for polarized NH_3(left) and ND_3(right)

3.3 Running Conditions

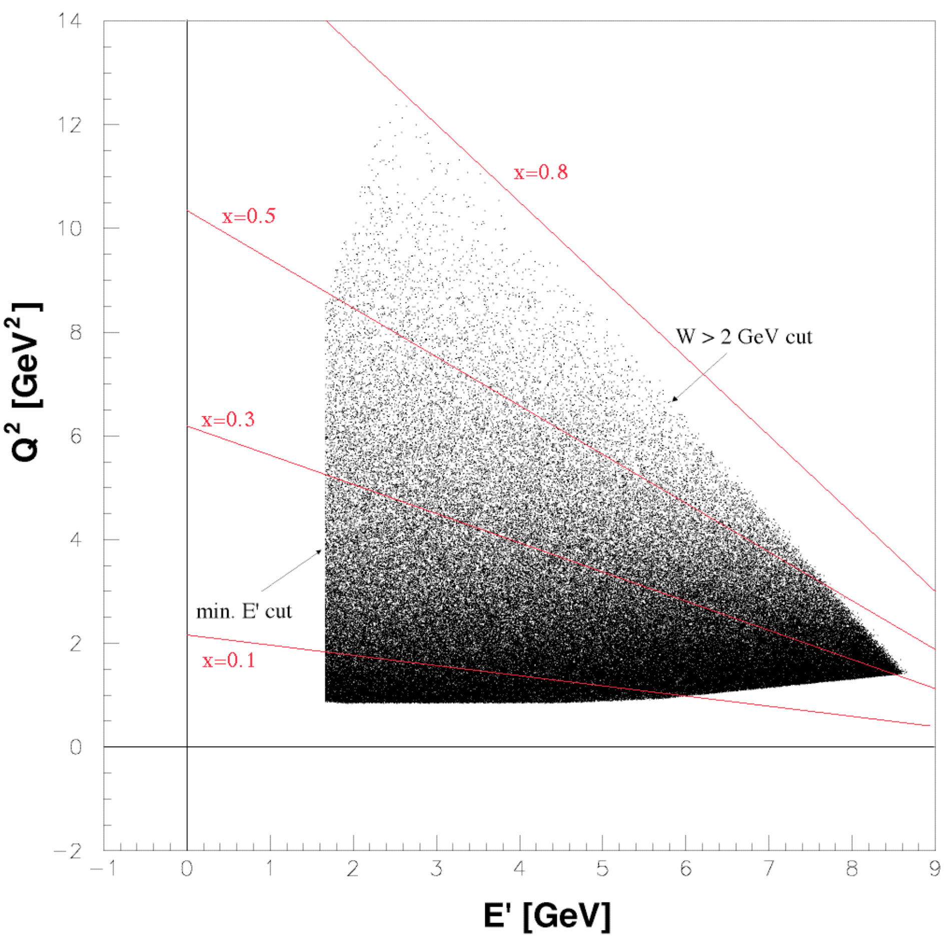

Figure 22: Kinematic coverage in the DIS region of the proposed experiment.

We will run with a beam of about 10 nA on a 3 cm long ammonia target, resulting in a luminosity of $10^{35}/\text{cm}^2\text{s}$. The beam will be rastered over the diameter of the polarized target (about 3 cm) to minimize the dose density (we will need at most one anneal every other day under these conditions). We assume a beam polarization of 0.85, which has been routinely achieved in recent experiments running at Jefferson Lab. The beam helicity will be flipped in a pseudo-random pattern every 33 ms. We will use the standard Hall B beam devices to monitor and stabilize the beam intensity and position. In particular, we will reduce any helicity-correlated beam asymmetries to less than 10^{-3}.

The first-level trigger will consist of a coincidence between the high-threshold Cherenkov counter and a signal above threshold (corresponding to at least 1 GeV deposited) in the electromagnetic calorimeter in the same sector. This trigger will be highly specific for high-energy electrons, with little contamination from pions and other particles. In the case of too high background, we can also implement a level 2 trigger which requires a electron candidate track in the drift chambers of the same sector as the level 1 trigger. This has already been developed for the present CLAS. The total event rate in the DIS region for this experiment is expected to be around 2000 Hz above $Q^2 = 1$ GeV^2. Estimates of the total trigger rate are around 20 kHz. A data acquisition rate of 10 kHz has already been achieved with today's technology for the present CLAS DAQ, so that the required data acquisition rate for this experiment is a rather modest extrapolation.

In Fig. 22 we show the kinematic coverage in the DIS region expected from the proposed experiment with 11 GeV beam and CLAS12. Clearly this will constitute a substantial increase over the existing Jefferson Lab data in both x and Q^2 (maximum Q^2 of 5 GeV^2 and x between 0.2 and 0.6), while the precision of the expected data will be far superior to existing DIS experiments from other labs. In addition, we will also cover the elastic/quasi-elastic and resonance region, with the potential to study inclusive resonance excitation and local duality at high Q^2.

3.4 Analysis

3.4.1 Extraction of asymmetries

The data will consist of the number of counts for beam helicity antiparallel (N^+) and parallel (N^-) to the longitudinal target polarization, each normalized to the dead-time corrected integrated beam charge. We will subtract from these rates the backgrounds from misidentified pions (which can be obtained from fits to the distribution of photo-electrons in the high-threshold Cherenkov counter and the measured ratio of visible energy deposited in the electromagnetic calorimeter to the measured momentum) and from electrons coming from pair-symmetric decays (e.g., $\pi^0 \to e^+e^-$ or $\pi^0 \to \gamma e^+e^-$ as well as $\gamma \to e^+e^-$ conversions). From the corrected counts, we will form the ratio $A_{||}^{raw} = (N^+ - N^-)/(N^+ + N^-)$. This ratio has to be divided by the product of beam and target polarization and the dilution factor (the fraction of counts coming from the polarized nuclei in the target to the total).

The dilution factor can be calculated from a detailed model of the target content and a parametrization of the world data on unpolarized structure function for nucleons and nuclei (^{15}N, ^{4}He, and C and Al foils) in the target, including radiative effects. The only ingredient needed is the packing fraction (the fraction of the cell volume occupied by the ammonia beads), which can be extracted by comparing the rate from ammonia to that from an auxiliary carbon target. Additional measurements on empty and liquid-helium only targets will also be needed. Past experience with the EG1 experiment in Hall B have shown that a typical error of 3% on the dilution factor can be achieved [15]. An additional correction for the small polarization in ^{15}N and contamination by ^{14}N and, in the case of the deuterated ammonia, H, will be applied as well.

The beam (P_B) and target (P_T) polarization will be independently measured using Möller scattering and NMR, respectively. However, we can extract the product $P_B * P_T$ with higher precision directly from our data, by measuring the asymmetry of elastic (quasielastic) scattering $\vec{p}(\vec{e}, e'p)$ ($\vec{d}(\vec{e}, e'p)$) from our NH_3 (ND_3) targets, respectively. We did a full simulation of this method, including radiative effects, CLAS12 acceptance and expected beam parameters. We find that the uncertainty on $P_B * P_T$ for the proton will be about 1% and on the deuteron about 3%.

As a final step, we will correct the asymmetry $A_{||}$ for both external and internal radiative effects, following the method by Kuchto and Shumeiko [46] for the internal corrections and by Mo and Tsai [47] for the external corrections. The existing code is very mature and well-tested and should yield systematic errors on the extracted asymmetries of 3% (relative) on average, including uncertainties due to the model input for all structure functions (for which an extensive data set at lower Q^2 and W has been collected by all three Halls at Jefferson Lab).

3.4.2 A_1 and g_1

The final result after all steps outlined above is the longitudinal (Born) asymmetry $A_{||} = D(A_1 + \eta A_2)$ (see Section 1). The factor D depends on the ratio R of longitudinal to transverse photo absorption cross sections, which is well known after a series of detailed experiments in Jefferson Lab's Hall C. These experiments, which will be continued at 11 GeV, produce a very reliable fit for all unpolarized structure functions of the proton and the deuteron (F_1 as well as R), making the division by D straightforward.

The remaining unknown ingredient is the virtual photon asymmetry A_2. There are some results for A_2 from experiments in Hall C (on the proton and deuteron) and Hall A (on ^{3}He) as well as from SLAC at higher Q^2. At low W, fits to exclusive resonance production data such as the MAID parametrization can help constrain A_2. Further constraints come from upper bounds like the Soffer bound and the Burkhard-Cottingham sum rule. The EG1 experiment with CLAS can also provide some constraints on A_2, so that a fairly reliable model can be constructed to cover the region of interest. Fortunately, both the magnitude of A_2 and its contribution to the measured asymmetry $A_{||}$ will be small, so that even a rather crude model results in a reasonably small systematic error for the extracted asymmetry A_1 or the ratio of structure function g_1/F_1. For the present proposal, we have allowed for a conservative estimate of this systematic error, by assuming that the uncertainty on A_2 is comparable to its magnitude. This ranges from 10% relative error on the asymmetry at low x to less than 1% for our highest x point.

In any case, ultimately the precision of the data extracted from the proposed measurement will be improved by directly measuring A_2. This measurement requires a transversely polarized target, which is not part of the base equipment in Hall B and therefore not included in the present proposal. However, plans for such a target are fairly advanced and its construction has been recognized as an imperative addition to the base equipment. A future proposal will detail this target and the measurements to be made with it.

The final quantities to be extracted from our data are the spin asymmetry A_1 and the ratio of structure functions g_1/F_1 (which differs only by a small correction due to A_2, partially offset by the correction required to go from $A_{||}$ to A_1). The former quantity can be directly compared to models of the quark polarization in the limit of $x \to 1$. The latter is used directly as input for NLO analyses, which for consistency use unpolarized PDFs to compute the unpolarized structure function F_1. By using the rather precise parametrization for F_1 from the Hall C experiments mentioned above, we can also derive the spin structure function $g_1(x, Q^2)$. This quantity is needed to evaluate moments and for tests of duality.

4 Expected Results

4.1 Simulation

The expected number of counts and corresponding statistical errors in the following sections are based on a full simulation of inclusive and semi-inclusive inelastic scattering with the CLAS12 acceptance folded in. Events were generated with the clas12DIS generator written by H. Avakian and P. Bosted. This generator is basically an implementation of the LUND Monte Carlo package called PEPSI (Polarized Electron-Proton Scattering Interactions) [32]. It is based on polarized and unpolarized parton distribution functions and the LUND string model for hadronization, and has been tested successfully against several low-Q^2 experiments with 5.x GeV beam at Jefferson Lab.

A fast Monte Carlo simulation program (clasev) has been written by H. Avakian to model the acceptance and resolution of the CLAS12 detector with all of the standard (base) equipment in place. The events generated by clas12DIS are used as input and all particles are followed through all detector elements. The results of our simulation have been cross-checked with direct cross section calculations and a simple geometric acceptance model.

The resolution of the detector is simulated by a simple smearing function which modifies a particle's track by a random amount in momentum and angles according to a gaussian distribution of the appropriate width. The amount of smearing follows the design specifications of the CLAS12 detector. In Fig. 23 the resulting resolutions for the Bjorken variable x are shown as a function of x for various bins in Q^2. The resolution varies between $0.01 < \sigma_x < 0.035$ and is therefore finer than our planned x bin size of 0.05 in all cases. A full Monte Carlo simulation (GEANT4-based) of CLAS12 with all resolution effects will be used to determine the effective mean x (and Q^2) for each x-bin we will use to bin our data so we can accurately extract the x-dependence of the measured asymmetries.

4.2 Statistical and systematic errors

We base our predicted statistical errors in the following sections on the assumption of running 30 days on NH_3 and 50 days on ND_3. The number of days was chosen to achieve a statistical error that is not significantly larger than the systematical error at the highest x points. More days on deuterium than the proton ensures that both have the same statistical error at large x and optimizes the error on extracted quantities like $\Delta d/d$ and $\Delta g/g$ from NLO analyses.

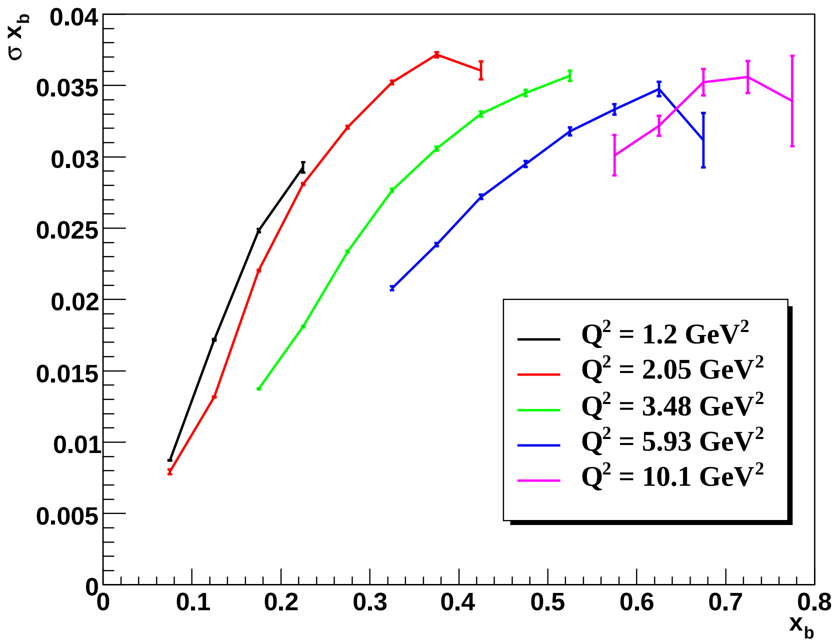

Figure 23: Expected resolution of the CLAS12 detector for x for a number of bins in Q^2. Errors reflect the uncertainty due to the fitting procedure only.

Systematic Error Source	Typical Value in % of Measured Asymmetry
False asymmetries	$< 1\%$
Background subtraction	$< 1\%$
Dilution factor	3 %
Product of beam and target polarization	1% (proton) and 3% (deuteron)
Radiative corrections	3%
Unpolarized structure functions	From 1% (A_1) to 5% (g_1 for the neutron)
Asymmetry A_2	From 1% (high x) to 10% (low x)
Total for A_1^p	5-6 % at high x, 6-11% at low x
Total for A_1^d	7% at high x, 10-20% at low x

Table 4: Summary of systematic error estimates.

For our estimate of the total systematic error, we have added the systematic errors from the various contributions discussed in the previous Section in quadrature. They are listed in Table 4. Note that some systematic errors (like the overall scale error coming from the beam and target polarization) affect the extraction of PDFs or higher twist contributions less than point-to-point errors, which typically are smaller. It should be understood that the ultimate systematic error of this experiment depends on our knowledge of unpolarized structure functions and A_2, which we can only estimate very roughly for an experiment many years in the future. In particular, the relatively large uncertainty due to A_2 will be all but eliminated by additional measurements with transversely polarized target planned for CLAS12.

4.3 Inclusive Spin Structure Functions

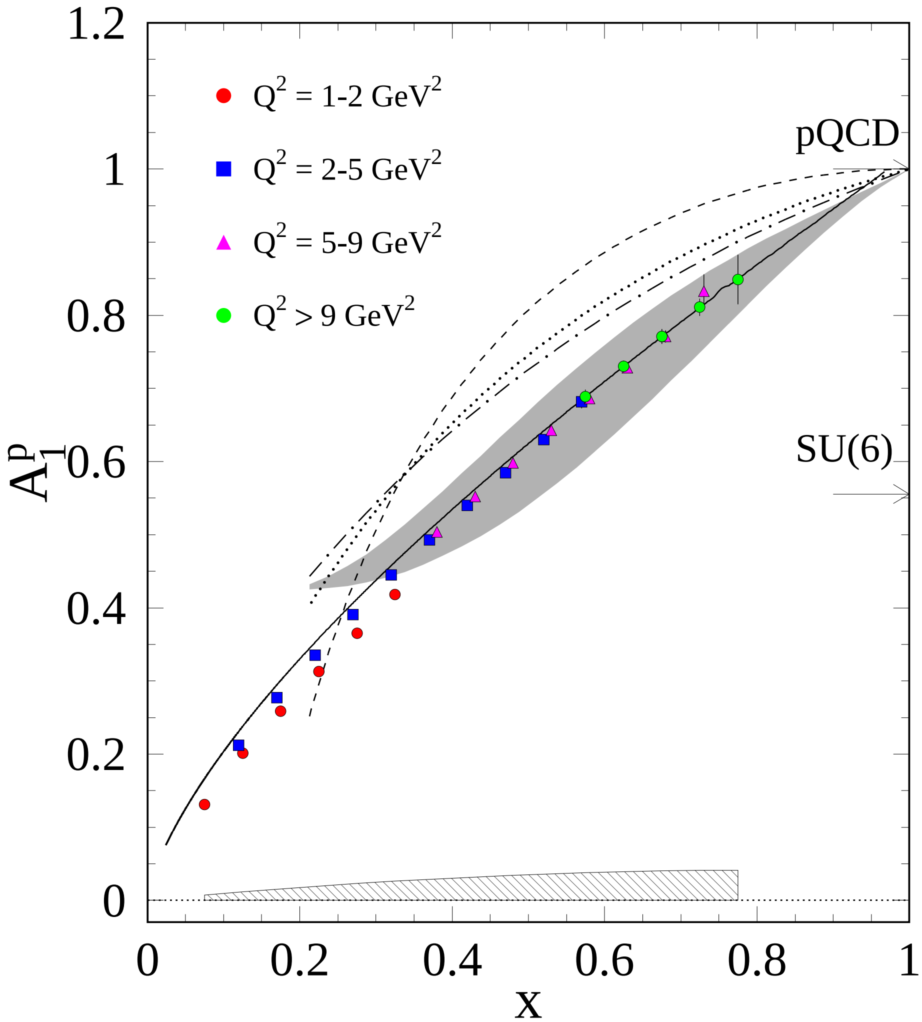

Figure 24: Expected results for the virtual photon asymmetry A_1^p measured with CLAS12. The four different symbols correspond to 4 different Q^2 ranges. Error bars are statistical only, while systematic errors are shown by the shaded region close to zero. Some of the models discussed in the Physics Motivation section are shown for comparison (see text for explanation).

In Figures 24 and 25 we show the expected precision for the proposed measurements of the inclusive virtual photon asymmetry A_1 for the proton and the deuteron. We show simulated data for each of 4 ranges in Q^2 accessible with 11 GeV beam. The lowest x point for each Q^2 range is determined by the minimum scattering angle accessible with CLAS12,

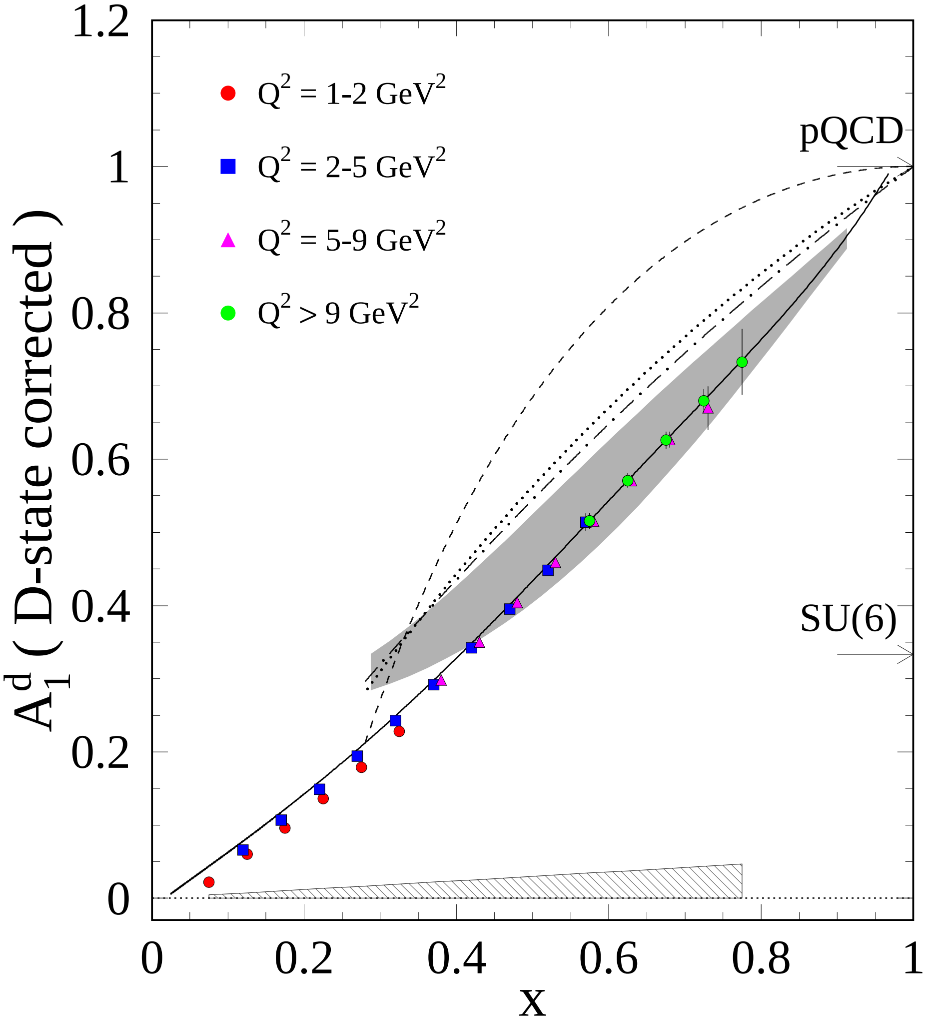

Figure 25: Expected results for the virtual photon asymmetry A_1^d measured with CLAS12. Symbols and curves are as in the previous figure. All model curves are for an "isoscalar nucleon" while the simulated experimental data have been divided by the D-state correction $(1 - 1.5 w_D)$.

while the highest x point is determined by the maximum scattering angle (about 40°) and the requirement that the missing mass of the unobserved final state, W, be larger than 2 GeV. If one assumes that the asymmetry $A_1(x, Q^2)$, averaged over a range in W below 2 GeV, agrees with $A_1(x, Q^2)$ at some higher Q^2 and in the DIS region ($W > 2$ GeV) ("local duality"), one could lower this limit and correspondingly extend the reach in x of this experiment (up to about $x = 0.9$). Except for the lowest and the highest x points, we will have several Q^2 bins for each x. Together with the existing DIS data from high-energy labs like SLAC, CERN and DESY, this coverage in Q^2 will facilitate NLO analyses and determinations of the Q^2-dependence of spin structure function moments.

The solid line in each figure is a parametrization of the high energy world data [8] at an average Q^2 of 10 GeV^2. The deviation of the simulated data points from this line and from each other takes into account our best present knowledge of scaling violations (Q^2-dependence of $A_1(x)$). The error bars (too small to be visible at lower x) indicate the expected statistical uncertainty, while the band at the bottom of each plot are our estimate of the systematic error. Since a major goal of this experiments is the exploration of the limit $x \to 1$ of the asymmetry $A_1(x)$, we have based our beam time request on the combined error achievable for the highest x values. However, the vast statistics to be collected at intermediate x will, at the same time, provide very good constraints on NLO analyses of our data.

The remaining lines and shaded band in Figs. 24 and 25 correspond to some of the models discussed in Section 2 of this proposal. The three lines are from the three different versions of the model in [18], with the SU(6) symmetry-breaking mechanism assumed to be helicity-1/2 dominance (dashed), spin-1/2 dominance (dotted), and symmetric wave function suppression (dash-dotted), respectively. The shaded band covers the range of predictions by the hyperfine-perturbed quark model [16]. The arrows indicate the (constant) value according to SU(6) symmetric quark models.

It is obvious from Figs. 24 and 25 that our data will not only exceed very clearly the SU(6)-symmetric value for A_1, but also will be able to unambiguously differentiate between several possible mechanisms for the SU(6) symmetry breaking. In particular, models which assume that the struck quark helicity is equal to the nucleon helicity (as predicted by pQCD and as shown by the top-most model lines in the figures) can be clearly distinguished from models where d/u tends to zero but the d-quark polarization stays negative up to the highest x (bottom line and shaded band in the figures).

This can be seen even more clearly from Fig. 26 where we have used a simple LO approximation to "extract" the down-quark polarization $\Delta d/d$ from our simulated data on the proton and the deuteron under two different assumptions for $\Delta d/d(x \to 1)$. Once the real data are in hand, we will of course rely on a complete NLO analysis (including higher twist effects) to determine the precise value of $\Delta d/d$ at all x. However, Fig. 26 illustrates the discriminating power of our expected data. While all existing data are compatible with a constant value of about $-1/3$ for the d-quark polarization in the valence region, they cannot exclude a "late rise" towards $\Delta d/d \to 1$, while our new data would clearly show such a rise at large x.

For a more complete picture of the precision for polarized parton distribution functions achievable with our expected data, we have plotted in Fig. 27 an analysis of the impact these data would have on NLO analyses. The outermost envelopes on each panel correspond to the present uncertainty from all world data excluding the recent EG1b results with CLAS [15].

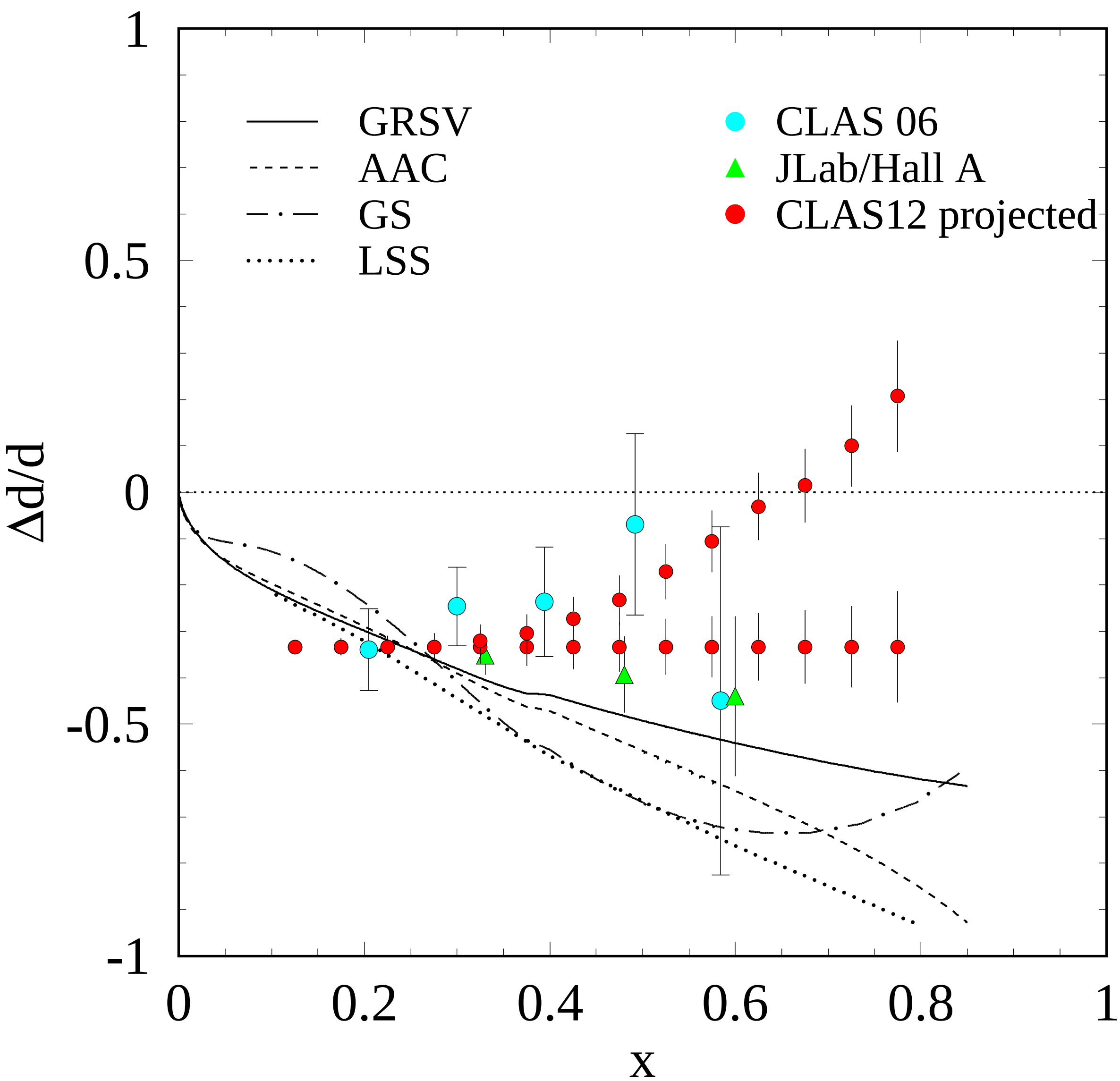

Figure 26: Expected results for the polarization $\Delta d/d$ of d-quarks in the proton extracted from the asymmetries A_1^p and A_1^d measured with CLAS12. CLAS12 "data" points are shown both for the case $\Delta d/d = -1/3 = const.$ and for the case where $\Delta d/d \to 1$ as $x \to 1$. The actual shape of the distribution for $\Delta d/d$ is unknown and the second set of "data" points follows an arbitrary curve chosen for illustrative purposes only. Error bars include statistical and point-to-point systematic errors combined. Similarly extracted results from existing JLab data (EG1b and HallA) are also shown for comparison.

After inclusion of these data, the uncertainties will reduce to the middle envelope (dashed line). This improvement is due both to the contribution of CLAS to the world DIS data directly and also to a very much improved determination of higher twist effects which are important at Jefferson Lab energies but also influence data taken at SLAC and DESY.

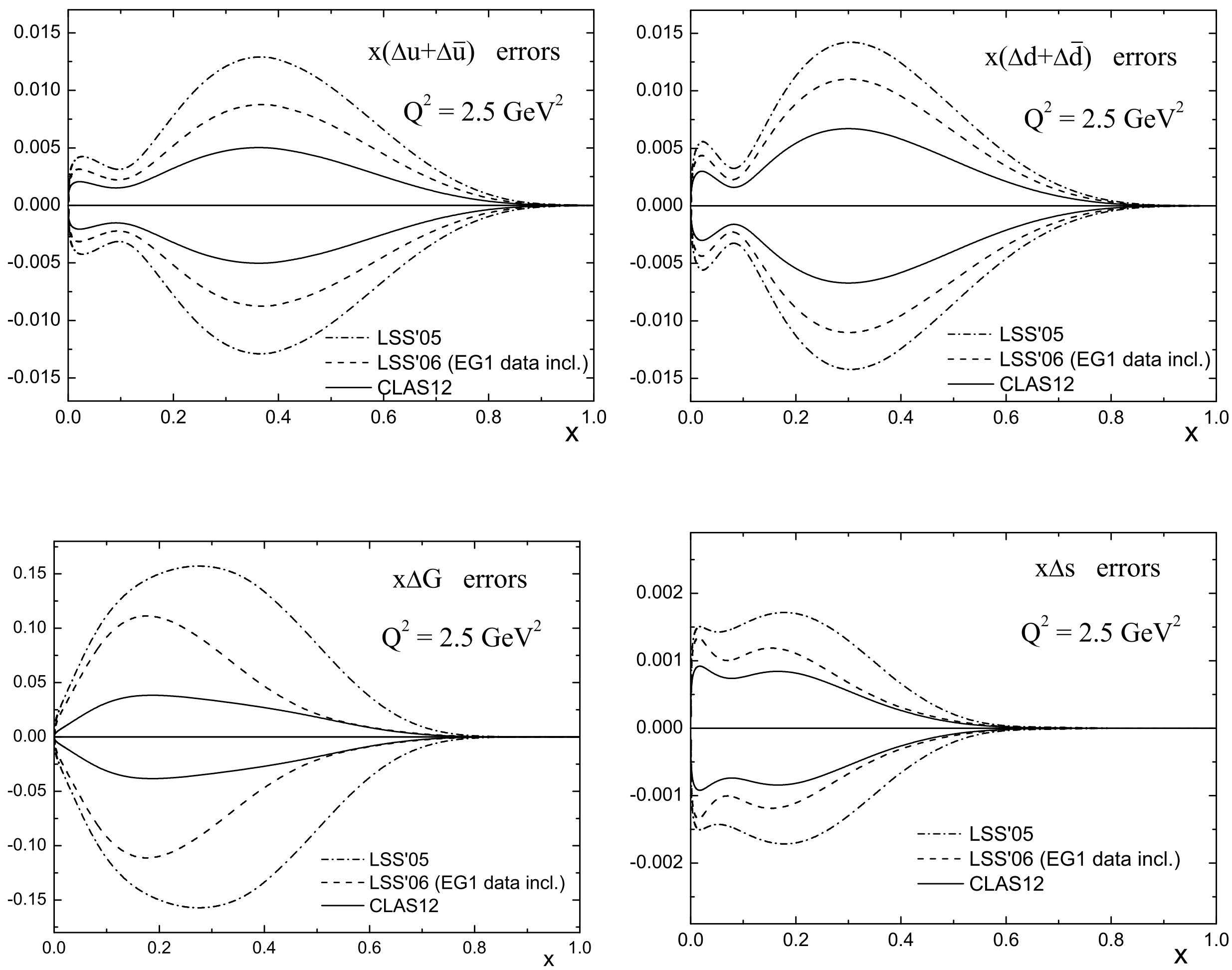

Figure 27: Expected uncertainties for polarized quark distributions Δu, Δd, ΔG and Δs from a NLO analysis of all world data. The outermost line shows the result from a recent analysis by Leader, Sidorov and Stamenov [23]. The second line is the updated result from these authors after inclusion of the new EG1b data from CLAS at 5.7 GeV [15]. The innermost line shows the expected uncertainty after including the data set to be collected with this experiment, including statistical and systematic errors.

A dramatic further improvement (solid line, innermost envelope) can be achieved with the expected data from the experiment proposed here. Surprisingly, this improvement affects not only the valence Δu and Δd quark distribution (which are the main goal of the proposed experiment), but even the polarized gluon distribution ΔG at moderate to high x. This is due to the fact that, in particular for the asymmetry on the deuteron, its Q^2-dependence in this x range is mostly driven by the gluon distribution. The improvement for strange quarks is less impressive, since the x range we cover doesn't extend much below $x = 0.1$ where strange quarks dominate.

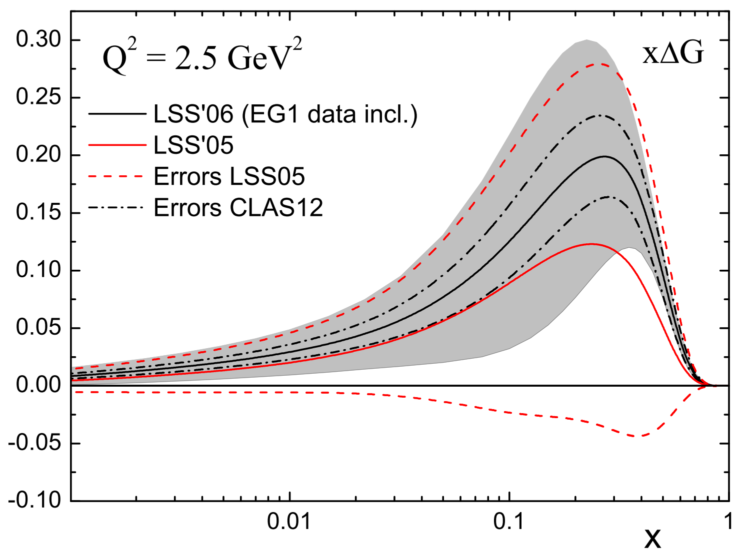

Figure 28: Illustration how our knowledge of ΔG would be affected by the data from the proposed experiment.

The knowledge we can gain on ΔG is further illustrated in Fig. 28. Here the red solid line and the red dashed lines indicate our present knowledge of this PDF, before inclusion of the new CLAS data at 5.7 GeV. After adding these data to the world data set, the best fit moves to the solid black line, with much reduced errors as indicated by the grey band. Finally, the precision achievable with the expected data at 11 GeV is indicated by the dash-dotted lines. One should emphasize that our data will not only reduce the error band on ΔG but will likely allow a more detailed modeling of its x-dependence, which may well be oscillating in sign (as indicated by recent RHIC data). By combining our inclusive results with direct measurements of ΔG expected from RHIC and COMPASS, we will finally be able to pin down the contribution of the gluon helicity to the overall nucleon spin to a precision comparable to our knowledge of the quark spin contribution, $\Delta\Sigma$.

Part of the improvement expected for the polarized PDFs comes from a much better determination of higher twist contributions to the spin structure functions that potentially affect all data. Using the ansatz by Leader, Sidorov and Stamenov [23], one can understand the measured spin structure function $g_1(x, Q^2)$ as a sum of a leading twist term $g_1(x, Q^2)_{pQCD}$ and a higher twist term, which to first order can be written as $h(x)/Q^2$ (see section 2.1). Only after subtracting this term can one use measured g_1 data as input to a NLO analysis. We show in Fig. 29 the present knowledge of this higher twist term $h(x)$ for the proton and the neutron, and the expected improvement of this knowledge once results from this experiment are available. These improvement is rather impressive, especially at lower x (where the

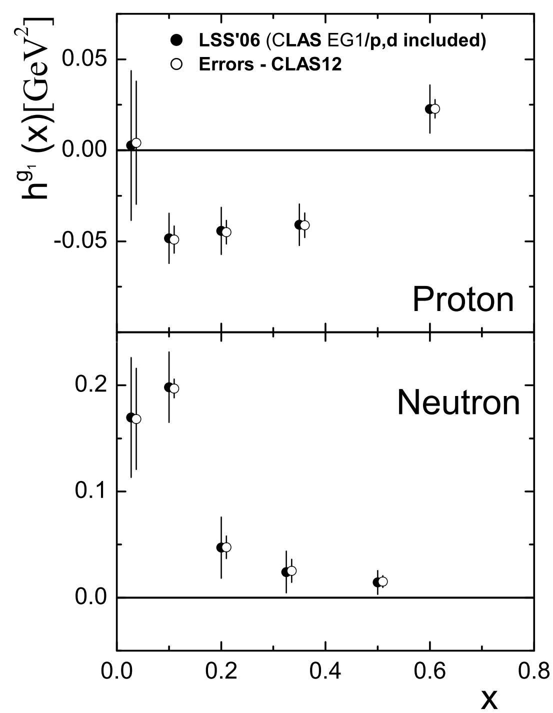

Figure 29: Illustration how our knowledge of higher twist corrections to spin structure functions would be affected by the data from the proposed experiment.

existing CLAS data have little coverage) and for the neutron, which can be extracted from our proposed high-statistics run on deuterium. Present analyses show very large HT effects around $x \approx 0.1$ for the neutron (see Fig. 29), albeit with large error bars. If this trend is confirmed with the much more precise data expected from the proposed experiment, it might lead to a *decrease* of the asymmetry A_1 for the deuteron with increasing Q^2, as already indicated in Fig. 9.

4.4 Semi-inclusive Results

As outlined in Section 2, the proposed experiment will simultaneously collect data on inclusive asymmetries in $\vec{p}, \vec{d}(\vec{e}, e')$ as well as asymmetries for the semi-inclusive channels $\vec{p}, \vec{d}(\vec{e}, e'\pi^{+,0,-})$. The charged pions will be detected in the forward spectrometer and the central tracker of CLAS12 in coincidence with the scattered electrons. The following predicted results were obtained with a full simulation of the hadronization process [32] and the acceptance of CLAS12 for all particles.

In addition to the backgrounds already discussed earlier, for the pion production channel we will have to consider contributions from diffractive vector meson production (e.g., $\rho \to \pi\pi$) and the radiative tail on exclusive pion production. For the NLO analysis, we also need to know the unpolarized cross section for SIDIS pion production, which will be measured in several Hall C experiments (both with the present 6 GeV beam and also with the upgraded CEBAF). The contributions to the systematic error from these backgrounds requires a detailed analysis once the requisite data are in hand, but experience with EG1 data from CLAS at 6 GeV show that one can avoid most of them by judicious choice of kinematic cuts.

Q^2	x	$A_{\|\|p}^{\pi^+}$	$A_{\|\|p}^{\pi^-}$	$A_{\|\|d}^{\pi^+}$	$A_{\|\|d}^{\pi^-}$
1.5	0.075	0.0004	0.0005	0.0005	0.0006
1.5	0.125	0.0004	0.0005	0.0005	0.0006
1.5	0.175	0.0006	0.0007	0.0007	0.0009
1.5	0.225	0.0008	0.0010	0.0009	0.0012
1.5	0.275	0.0010	0.0012	0.0011	0.0015
1.5	0.325	0.0013	0.0016	0.0015	0.0019
3.5	0.125	0.0008	0.0010	0.0010	0.0012
3.5	0.175	0.0006	0.0008	0.0007	0.0009
3.5	0.225	0.0006	0.0008	0.0008	0.0010
3.5	0.275	0.0007	0.0009	0.0008	0.0011
3.5	0.325	0.0008	0.0011	0.0010	0.0013
3.5	0.375	0.0009	0.0012	0.0011	0.0014
3.5	0.425	0.0012	0.0016	0.0014	0.0019
3.5	0.475	0.0017	0.0021	0.0020	0.0026
3.5	0.525	0.0026	0.0032	0.0031	0.0039
3.5	0.575	0.0051	0.0060	0.0061	0.0072
7.5	0.375	0.0021	0.0027	0.0025	0.0032
7.5	0.425	0.0021	0.0028	0.0025	0.0034
7.5	0.475	0.0023	0.0031	0.0027	0.0037
7.5	0.525	0.0026	0.0035	0.0031	0.0042
7.5	0.575	0.0032	0.0041	0.0038	0.0049
7.5	0.625	0.0043	0.0055	0.0051	0.0065
7.5	0.675	0.0074	0.0111	0.0088	0.0133
7.5	0.725	0.0139	0.0185	0.0167	0.0221
9	0.575	0.0095	0.0107	0.0114	0.0128
9	0.625	0.0087	0.0133	0.0104	0.0160
9	0.675	0.0099	0.0122	0.0119	0.0146
9	0.725	0.0128	0.0172	0.0154	0.0206

Table 5: Absolute statistical errors expected for longitudinal SIDIS asymmetries measured with CLAS12.

Table 5 contains the expected statistical uncertainties for the double spin asymmetries $A_{||}(x, Q^2)$ for each of the two targets and the two charged pion states. Here we have integrated over all SIDIS events with $z \geq 0.3$, yielding an average z of 0.6. The asymmetries themselves can range anywhere from zero (or negative) values up to 0.7 for the highest values in x. At lower x, this very large data set allows us to further subdivide the data into bins in p_T and z.

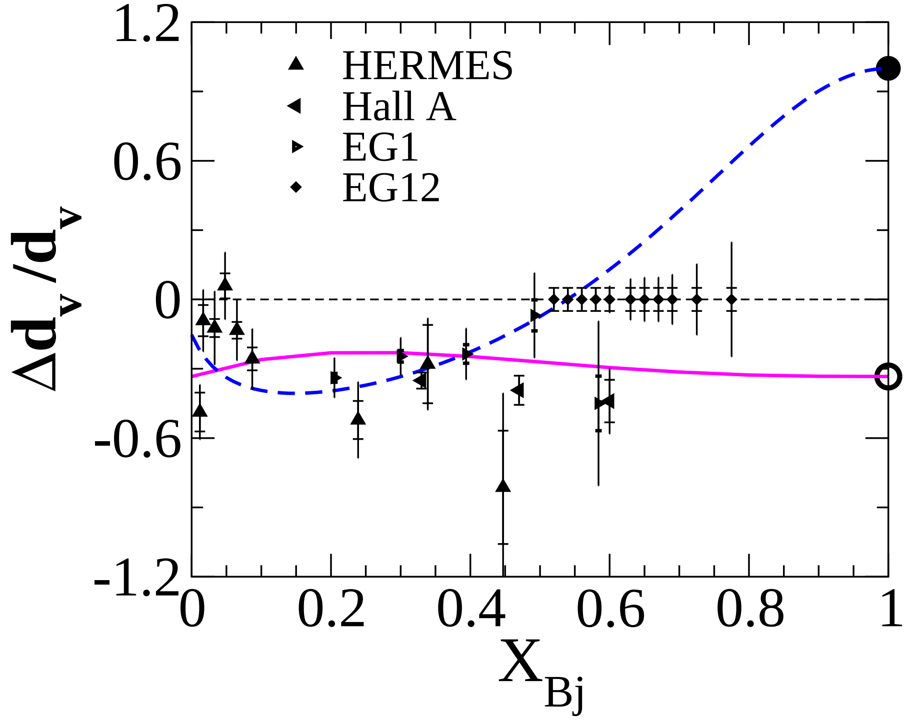

Figure 30: The polarization of valence down quarks ($\frac{\Delta d_V}{d_V}$) in the nucleon. The accuracy of future measurements appears on the zero line using Eq. 12 and the d/u ratio from [48]. Statistical errors are shown using the length of the error bar and the systematic uncertainties are shown using the riser of the error bars. Our data will extend to lower x than shown, down to $x \approx 0.1$, but systematic errors (which stay roughly constant with x) will completely dominate statistical ones in that region Recent data from HERMES [31] are shown for comparison. Also shown are the Hall A and EG1 results which used inclusive measurements to extract $\frac{\Delta d}{d}$. The solid curve represents a calculation using hyperfine perturbed quark wave functions [16] and the dashed line uses pQCD constrained fits to the world data set without the Hall A and EG1 results.

Once in hand, these data will be combined with existing SIDIS data from SMC, HERMES, COMPASS and RHIC for a full NLO analysis, including existing inclusive DIS data and those expected from this experiment. From this analysis, we will extract the polarized PDFs for each quark and antiquark flavor in the region $0.1 \leq x \leq 0.8$.

To illustrate the expected precision for the flavor-separated quark polarization from the proposed experiment, we used the approach of Eq. 12 to determine $\frac{\Delta d_V}{d_V}$ from the predicted rates of π^+ and π^- production off proton and deuteron targets as a function of relative beam and target spin. The results are shown in Fig. 30, together with existing HERMES SIDIS results and the inclusive data from Hall A. The error bars in this plot were calculated using a fit for the ratio $\frac{d}{u}$ as reported in Reference [48]. We assume that in the future $\frac{d}{u}$ will be known to about 5-10% in the region covered by our data (see the "BoNuS12" proposal to PAC30).

The expected data shown in Figure 30 are comparable with the precision achievable from the inclusive DIS measurement as seen in Fig. 26, although the statistical error will be larger at large x. On the other hand, the information from the SIDIS measurement is complementary to that from inclusive DIS; in particular at somewhat lower x where the contribution from anti-quarks is no longer negligible, only the SIDIS method can cleanly extract the valence quark behavior. In addition, SIDIS data depend in a somewhat different way on the assumption of isospin symmetry than DIS data, so a comparison between the two data sets could potentially uncover large violations of that symmetry. The SIDIS measurements proposed here can, all by themselves, clearly distinguish between the pQCD prediction of unity for $\frac{\Delta d_V}{d_V}$ when $x \to 1$ and the negative value predicted by the hyperfine perturbed constituent quark model [16]. In contrast, existing data have yet to indicate a trend towards a positive value for $\frac{\Delta d}{d}$ for large x. At lower x, our data will lead to much improved tests of isospin differences in the polarized sea ($\Delta\bar{u} - \Delta\bar{d}$) and, in a combined NLO analysis of all DIS and SIDIS data, to a much better determination of PDFs for each individual quark flavor.

4.5 Integrals and Sum Rules

To estimate the achievable statistical precision on Γ_1^p and Γ_1^d, we used the parameterizations of $F_2^p(x, Q^2)$ and $R(x, Q^2)$ from M.E. Christy [49] in the resonance region and the NMC [50] and E143's R1998 [51] fits for the DIS domain. We used the QFS model [52] for the deuteron and ^{15}N unpolarized cross sections. The longitudinal asymmetries were estimated using the parameterizations from S. Simula *et al.* [53] for the proton and from Bianchi and Thomas [54] for the proton and neutron that make up the deuteron. Figure 31 shows the expected statistical precision on the measured part of Γ_1^p, as well as results from HERMES [55] (green open triangles), SLAC E143 [56] (light blue diamonds) and E155 [57] (blue open star). The inner error bar is statistical while the outer one is the statistical and systematical uncertainties added in quadrature. Published results from CLAS EG1a [10] and preliminary results from EG1b (blue open squares) are also displayed for comparison. Like the CLAS12 data, the EG1 data do not include the unmeasured DIS contribution. The hatched blue band corresponds to the expected systematic uncertainty on the EG1b data points. The red band indicates the estimated systematic uncertainty (of about 5%) from CLAS12.

To obtain the uncertainty on the low-x extrapolation, we estimated the strength of the missing part of the integral using the model from Bianchi and Thomas [54], varying each parameter within the uncertainty range prescribed in [54] and adding in quadrature the propagated resulting uncertainties. This amounts typically to a 20% uncertainty on the missing strength for the proton and from 20% to 70% for the deuteron. This is a rather conservative estimate compared, e.g., to thepreliminary uncertainties quoted for the present EG1b data.

Not included in our uncertainty estimate is fact that data on A_2 will not be taken during this run. However, a subsequent transversely polarized target program is planned for CLAS12. In any case, transverse data from Hall B (from a transverse run or LT separation of the whole set of data) and the Hall C RSS [59] experiment and its extensions to 11 GeV will constrain well our knowledge of the contribution from A_2 to Γ_1. Precise transverse data in DIS were also taken by SLAC experiment E155x [60]. We also assumed that the structure functions $F_2^p(x, Q^2)$ and $R(x, Q^2)$ are known well enough at intermediate and large Q^2 thanks to SLAC and Hall C data, so that their contributions to the systematic uncertainty is small.

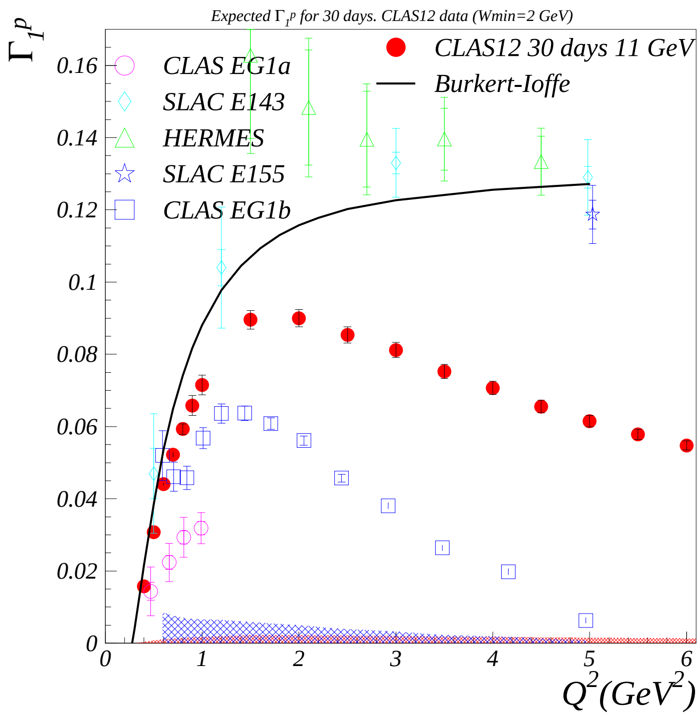

Figure 31: Expected precision on Γ_1^p for CLAS12 and 30 days of running (red circles). CLAS EG1a [10] (pink open circles) data and preliminary results from EG1b (blue open squares) are shown for comparison. The data and systematic uncertainties do not include estimates of the missing DIS contribution. The hatched blue band is the expected full systematic uncertainty on the EG1b and the red band is the systematic uncertainty expectation for CLAS12. HERMES [55] data (green open triangles) and SLAC E143 [56] and E155 data [57] (light blue diamonds and blue open star) are also shown. These data include DIS contribution estimates. The phenomenological model is from Burkert and Ioffe [58].

Figures 32 and 33 show the expected results on Γ_1^p and Γ_1^d including an estimate of the unmeasured DIS contribution. The systematic uncertainties for EG1 and CLAS12 here include the estimated uncertainty on the unmeasured DIS part. As can be seen on Fig. 32 and 33, moments can be measured up to $Q^2 = 6$ GeV^2 with a statistical accuracy improved several fold over that of the existing world data.

The higher Q^2 coverage and the expected high statistical accuracy will allow us to extract higher twist coefficients with great accuracy. These coefficients are related to OPE matrix elements which can give us information on the quark-gluon correlations in the nucleon. For instance, the matrix element f_2 is related to the polarizability of the color-electric and color-magnetic gluon field in the nucleon. As we already stated, the surprising smallness of the overall higher twist effects requires precise measurements at relatively large Q^2 (typically greater than 1 GeV^2. Staying above $Q^2 \simeq 1$ GeV^2 avoids the problem of the twist series convergence and of the rapidly increasing uncertainty in α_s. As a quantitative illustration of the impact of CLAS12, we extracted the expected twist-4 term f_2^{p-n} for the Bjorken

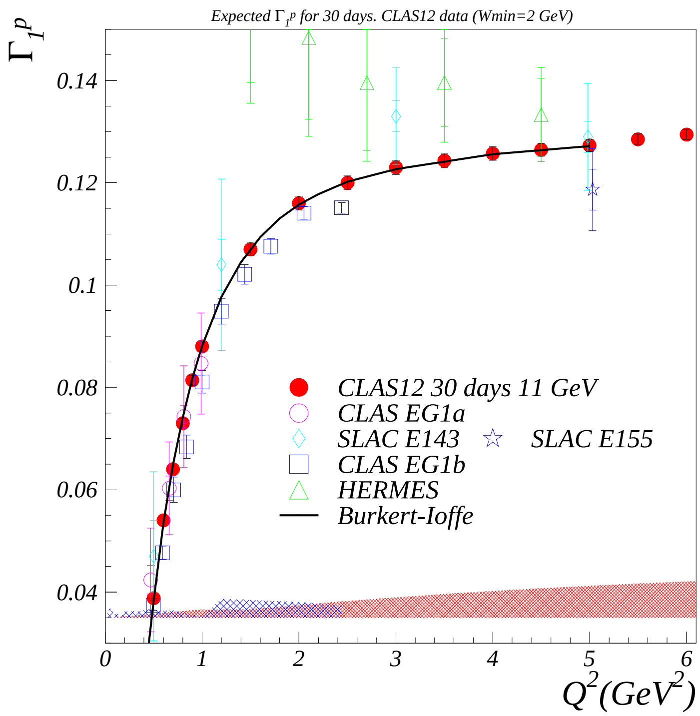

Figure 32: Expected accuracy on Γ_1^p for CLAS12 and 30 days of running (red circles). The CLAS12 and EG1 data and systematic uncertainties now include an estimate of the DIS contribution. The rest of the figure is the same as in Fig. 31 (note the different vertical scale).

sum using our expected statistic and systematic uncertainties and the same procedure as in Ref. [61]. At first order, the higher twist series for the Bjorken sum reads:

$$\Gamma_1^{p-n} = \frac{g_A}{6}\left[1 - \frac{\alpha_s}{\pi} - 3.58\left(\frac{\alpha_s}{\pi}\right)^2 - 20.21\left(\frac{\alpha_s}{\pi}\right)^3\right] + \frac{\mu_4^{p-n}}{Q^2} + ...$$

The term f_2^{p-n} is the twist-4 part of the $1/Q^2$ correction term:

$$\mu_4^{p-n} = \frac{M^2}{9}\left(a_2^{p-n} + 4d_2^{p-n} + 4f_2^{p-n}\right),$$

where a_2^{p-n} is the target mass correction given by the x^2-weighted moment of the leading-twist g_1 structure function, and d_2^{p-n} is a twist-3 matrix element given by

$$d_2^{p-n} = \int_0^1 dx\, x^2\left(2g_1^{p-n} + 3g_2^{p-n}\right).$$

The same elastic form factor parameterization as in [61] was used to add the elastic contribution to the moments (see Fig. 34). We separated the point-to-point correlated systematic uncertainty from the uncorrelated ones assuming the same ratio as in the preliminary EG1b

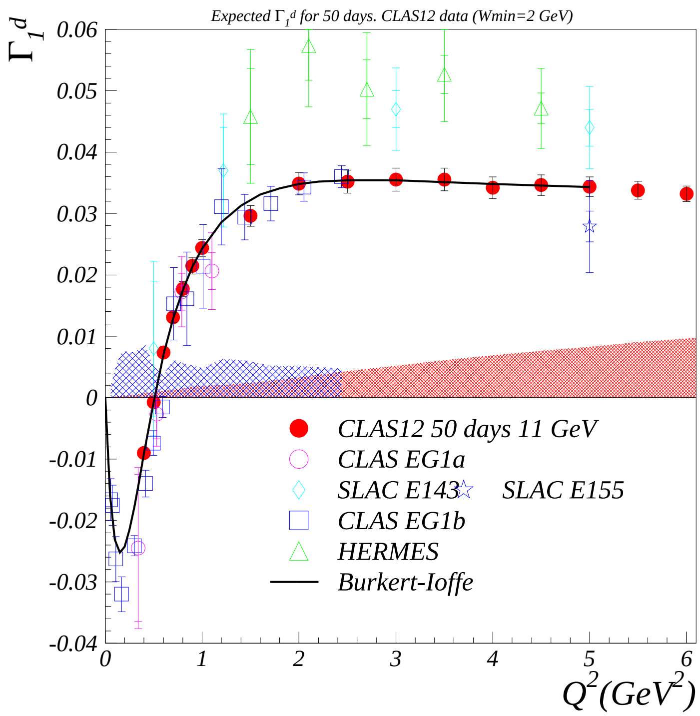

Figure 33: Same as figure 32 but for Γ_1^d and 50 days of running. The EG1a deuteron data is from Ref. [11].

higher twist analysis in which 30% of the systematic uncertainty is uncorrelated point to point. This point-to-point uncorrelated uncertainty is added in quadrature to the statistical uncertainty. Starting our extraction at $Q^2 = 1$ GeV^2, we find that our total uncertainty on f_2^{p-n} decreases by a factor 5.6 compared to results obtained in [61]. Even if we compare the expected precision on f_2^{p-n} with the fits in ref. [61] starting at $Q^2 = 0.66$ GeV^2 or $Q^2 = 0.81$ GeV^2 (which are more precise because they include the present JLab data), we still expect an improvement of a factor 2.4 to 2.7.

5 Summary and Request

The proposed set of measurements on polarized proton and deuteron targets will yield a comprehensive set of double spin asymmetries and polarized structure functions in a wide region of x and Q^2, up to the highest x reachable by any existing accelerator in the foreseeable future. These measurements will vastly improve on the precision and density of data points in the valence quark region for low to moderate Q^2. Our inclusive and semi-inclusive data, combined with the world data set, will allow us to extract significantly more precise polarized parton distributions, including the helicity carried by gluons in the nucleon. Finally, we can improve considerably on our knowledge of higher twist contributions to the moments of spin structure functions.

To achieve this goal, we request a total of 80 days of beam time with an 11 GeV, 10 nA

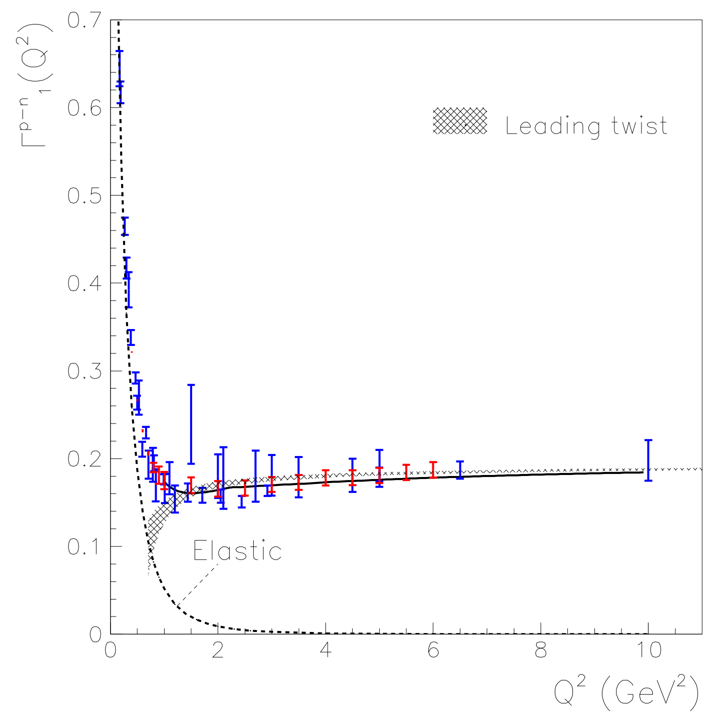

Figure 34: Extraction of the twist-4 term f_2^{p-n} from the expected CLAS12 data (in red) added to the published world data (in blue) for the Bjorken sum. The plain line is the result of a fit starting at Q^2=1 GeV^2 using a twist series truncated to order $\frac{\mu_4^{p-n}}{Q^2}$. The gray band is the pQCD NNLO leading twist evolution of the Bjorken sum. The elastic contribution to Γ_1^{p-n} is shown by the dashed line. The uncertainty on the CLAS12 points is the total point-to-point uncorrelated uncertainty. We expect to reduce by approximately a factor 6 the total point-to-point uncorrelated uncertainty compared to the result of ref. [61].

highly polarized electron beam in Hall B. The breakdown of this beam time is shown in Table 6. The number of days requested was chosen to optimize the impact of our data and to make the systematic and statistical errors roughly equal for the highest x data points.

We want to conclude by noting that while this experiment requires a substantial commitment of beam time (80 days total), many different scientific questions can be addressed by these data at the same time. In addition to the various channels (DIS and SIDIS) described in detail in the present proposal, we will also simultaneously take data on Deeply Virtual Compton Scattering (described in a separate proposal to PAC30) and other deep exclusive processes, like meson production. In these experiments, target asymmetries are complementary to beam spin asymmetry measurements and allow a better untangling of the various Generalized Parton Distributions of the nucleon.

In addition, the proposed experiment will yield data on single (target) spin asymmetries in SIDIS (which can provide constraints on the Sivers and Collins effects and higher-twist nucleon structure functions - see the LOI submitted to this PAC [28]) and high-Q^2 data in the resonance region (both inclusive and exclusive with detection of a final state meson like

Time	Activity
3 days	Commissioning: Beam raster set up, trigger optimization, low energy calibration runs
24 days	Production data taking on NH_3
40 days	Production data taking on ND_3
3 days (1 1/2 hours every other day)	Target anneals and/or target changes
10 days (intermittent with production data)	Calibration runs on ^{12}C and empty target
2 day (1 hour every other day – concurrent with anneals)	Möller polarimeter runs

Table 6: Requested beam time broken down by activity.

pion, eta, phi, rho etc.). These channels will likely become part of future proposals for the energy-upgraded CEBAF.

Finally, we want to mention several possible additions to the base equipment that will substantially enhance our physics reach. We already addressed the desirability for running with a transversely polarized NH_3 and ND_3 target. This option is under active investigation and will most likely lead to further proposals in the near future. With a transversely polarized target, we could not only reduce the systematic errors on A_1 and g_1, but also directly measure the second spin structure function g_2, and, via single spin asymmetries and the Collins effect, extract information on the transversity spin structure function (the third leading order structure function of the nucleon). We are also considering the addition of a Ring-imaging Cherenkov (RICH) to CLAS12, which would allow us to unambiguously separate kaons from pions and protons and therefore to get additional information on the quark flavor dependence of the nucleon spin structure functions. The present proposal can thus be considered the first major step in a large program which will completely map out the spin structure of the nucleon in the moderate to high-x region.

References

[1] AAC Collaboration, hep-ph/0603213.

[2] G. Baum *et al.* [E130 Collaboration], Phys. Rev. Lett. **51**, 1135 (1983).

[3] J. Ashman *et al.* [EMC Collaboration], Nucl. Phys. **B328**, 1 (1989).

[4] D. Adams *et al.* [Spin Muon Collaboration (SMC)], Phys. Lett. **B396**, 338 (1997).

[5] B. Adeva *et al.* [Spin Muon Collaboration (SMC)], Phys. Lett. **B412**, 414 (1997).

[6] K. Abe *et al.* [E143 collaboration], Phys. Rev. D **58**, 112003 (1998) [arXiv:hep-ph/9802357].

[7] K. Abe *et al.* [E154 Collaboration], Phys. Rev. Lett. **79**, 26 (1997) [arXiv:hep-ex/9705012].

[8] P. L. Anthony *et al.* [E155 Collaboration], Phys. Lett. **B493**, 19 (2000) [arXiv:hep-ph/0007248].

[9] A. Airapetian *et al.* [HERMES Collaboration], Phys. Rev. D **71**, 012003 (2005) [arXiv:hep-ex/0407032].

[10] R. Fatemi *et al.* [CLAS Collaboration], Phys. Rev. Lett. **91**, 222002 (2003).

[11] J. Yun *et al.* [CLAS Collaboration], Phys. Rev. C **67**, 055204 (2003).

[12] X. Zheng *et al.* [Jefferson Lab Hall A Collaboration], Phys. Rev. C **70**, 065207 (2004) [arXiv:nucl-ex/0405006].

[13] E. S. Ageev *et al.* [COMPASS Collaboration], Phys. Lett. **B612**, 154 (2005) [arXiv:hep-ex/0501073].

[14] S. S. Adler *et al.* [Phenix Collaboration], Phys.Rev.Lett. **93**, 202002 (2004).

[15] K. V. Dharmawardane, S. E. Kuhn, P. Bosted and Y. Prok [the CLAS Collaboration], to be published in Phys. Lett., arXiv:nucl-ex/0605028.

[16] N. Isgur, Phys. Rev. D **59**, 34013 (1999).

[17] N. Isgur, G. Karl and R. Koniuk, Phys. Rev. Lett. **41**, 1269 (1978); N. Isgur, G. Karl and R. Koniuk, Phys. Rev. Lett. **45**, 1738 (1980).

[18] F. E. Close and W. Melnitchouk, Phys. Rev. C **68**, 035210 (2003).

[19] F. E. Close and A. W. Thomas, Phys. Lett. **B212**, 227 (1988).

[20] G. R. Farrar and D. R. Jackson, Phys. Rev. Lett. **35**, 1416 (1975); G. R. Farrar, Phys. Lett. **B70**, 346 (1977).

[21] S. J. Brodsky, M. Burkardt and I. Schmidt, Nucl. Phys. **B441**, 197 (1995) [arXiv:hep-ph/9401328].

[22] M. Gluck, E. Reya, M. Stratmann and W. Vogelsang, Phys. Rev. D **63**, 094005 (2001) [arXiv:hep-ph/0011215].

[23] E. Leader, A. V. Sidorov and D. B. Stamenov, Phys. Rev. D **73**, 034023 (2006) [arXiv:hep-ph/0512114].

[24] J. Bluemlein and H. Boettcher, arXiv:hep-ph/0203155.

[25] M. Hirai, S. Kumano and N. Saito [Asymmetry Analysis Collaboration], Phys. Rev. D **69**, 054021 (2004) [arXiv:hep-ph/0312112].

[26] V. N. Gribov and L. N. Lipatov, Sov. J. Nucl. Phys. **15**, 138 (1972); Y. L. Dokahitzer, Sov. Phys. JETP. **16**, 161 (1977); G. Altarelli and G. Parisi, Nucl. Phys. **B126**, 298 (1977).

[27] C. Bourrely, J. Soffer and F. Buccella, Eur. Phys. J. **C23**, 487 (2002) [arXiv:hep-ph/0109160].

[28] H. Avakian *et al.*, "Semi-Inclusive Pion Production with a Longitudinally Polarized Target at 12 GeV", Letter of Intent to Jefferson Lab PAC 30, (2006).

[29] L. L. Frankfurt *et al.*, Phys. Lett. **B230**, 141 (1989).

[30] B. Adeva *et al*, Phys. Lett. **B420**, 180-190 (1998).

[31] A. Airapetian, Phys. Rev. D **71**, 012003 (2005) (hep-ex/0407032).

[32] L. Mankiewicz, A. Schafer, and M. Veltri, Comput. Phys. Commun. **71**, 305 (1992).

[33] K. Ackerstaff *et al.* Phys. Rev. Lett. **81**, 5519 (1998).

[34] E. Christova *et al.*, Phys. Lett. **B468**, 299 (1999).

[35] E. Christova and E. Leader, Nucl. Phys. **B607**, 369 (2001).

[36] D. de. Florian, C. A. Garcia Canal, R. Sassot, Nucl. Phys. **B470**,195 (1996).

[37] D. Graudenz, Nucl. Phys. **B432**, 351 (1994).

[38] V. Alexhakin *et al.* Phys. Rev. Lett. **94**, 202002 (2005).

[39] J.-P. Chen, A. Deur, Z.-E. Meziani, Mod. Phys. Lett. **A20**, 2745 (2005); M. Osipenko *et al.*, Phys. Rev. D **71**, 054007 (2005).

[40] J. D. Bjorken, Phys. Rev. **148**, 1467 (1966).

[41] S. D. Drell and A. C. Hearn, Phys. Rev. Lett. **16**, 908 (1966); S. Gerasimov, Sov. J. Nucl. Phys. **2**, 430 (1966).

[42] X. Ji and J. Osborne, J. Phys. **G27** 127 (2001).

[43] P. McKee, Nucl. Instrum. Meth. **A526**, 60 (2004).

[44] C. Dulya *et al.,* Nucl. Instr. and Meth. **354**, 249 (1995).

[45] C. Keith, Nucl. Instrum. Meth. **A501**, 327 (2003).

[46] T. V. Kukhto and N. M. Shumeiko, Nucl. Phys. **B219**, 412 (1983).

[47] Y.-S. Tsai, Rev. Mod. Phys. **46**, 815 (1974).

[48] W. Melnitchouk and A.W. Thomas, Acta Phys. Polon. **B27**, 1407 (1996) (nucl-th/9603021).

[49] M.E. Christy http://www.jlab.org/~christy/cs_fits/cs_fits.html.

[50] R. Arneodo *et al.* Phys. Lett. **B364**, 107 (1995).

[51] K. Abe *et al.* Phys. Lett. **B452**, 194 (1999).

[52] J. W. Lightbody, Jr. and J. S. O'Connell, Computers in Physics **2**, 57 (1988).

[53] S. Simula *et al.* Phys. Rev. D **65**, 034017 (2002).

[54] N. Bianchi and E. Thomas, Nucl. Phys. Proc. Suppl. **82**, 256 (2000).

[55] HERMES collaboration: A. Airapetian *et al.*, Eur. Phys. J. **C26**, 527 (2003).

[56] E143 collaboration: K. Abe *et al.*, Phys. Rev. Lett. **78**, 815 (1997); K. Abe *et al.*, Phys. Rev. D **58**, 112003 (1998).

[57] P.L. Anthony *et al.,* Phys. Lett. **B493**, 19 (2000).

[58] V. D. Burkert and B. L. Ioffe, Phys. Lett. **B296**, 223 (1992); J. Exp. Theor. Phys. **78**, 619 (1994).

[59] JLab E01-006, O. Rondon and M. Jones spokespersons. See also, e.g., K. Slifer, "The Hall C Spin Program at JLab", to be published in Czech. J. Phys., (2006).

[60] Anthony *et al.* Phys. Lett. **B553**, 18 (2003); Anthony *et al.* Phys. Lett. **B458**, 529 (1999).

[61] A. Deur *et al.* Phys. Rev. Lett.**93**, 212001 (2004).